Topics in marine hydrodynamics with numerical methods and MATLAB scripting

John Grue
Mechanics Division, Department of Mathematics, University of Oslo, Oslo, Norway
email: johng@math.uio.no
February 27, 2018

1 Lecture 1. Industries in the ocean environment

Current and future marine hydrodynamics applications relate to basically four types of industries, including:

1. Food production in the ocean environment
2. Transportation
3. Harvesting of offshore energy and marine mining
4. Infrastructure such as pipelines, road constructions in fjord crossings and other

Regarding the first category several constructions are being explored. They are thought to be located in the offshore environment which means that they will be exposed to wave forces. Both closed or open units are being considered where the closed ones have the advantage that they will not leak with potentially polluted water due to the fish farming. Open cages may be made of fish nets or of slotted media mounted to a fixed construction made of several beams.

* Illustration of potential fish cages and constructions for fish farming and aqua culture.

Shipping of goods by e.g. container ships, transportation of people on conventional or rapid ferries as well as the cruise industry are examples of the second category. Autonome ships, a recent innovation, recieves a particular interest because of potential new markets. Another example is ships for liquid natural gas (LNG) transportation where the wavy motion of the sea does not only enter in the calculation of the external forces on the vessel. However, the fluid motion of the LNG in the internal tanks of the ship needs also to be investigated and judged in the dimensioning and evaluation of the performance of the ship. The problem of sloshing in internal tanks moreover relate to land based transportation on both rail and road. Sloshing motion also occurs in tanks in air and space crafts.

* Illustration of container ships, rapid ferries, autonome ships, cruise ships, LNG-ship, sloshing in land based transportation and in space and aircrafts.

The offshore oil and gas industry are prominent examples of the third category. The production of the oil or gas may be performed from offshore platforms standing on the sea floor. Other production units may be floating platforms or ships. They are held in position by moorings or dynamical position systems. In the latter case one or more umbilicals connect the platform to the well at the sea floor. The constructions are built tall enough to have a positive air gap and clearing between the ocean waves and the production or living deck. Marine operations may be performed from special ships with a moon pool near its center where equipment is lowered into the water for the specific operations. Deep sea mining has been going on for decades with specialized ships and equipment.

A subsea development such as the Ormen Lange gas production unit is located on the sea floor at a depth of 1000 m.

Harvest of offshore wind energy is a new and growing industry where the construction supporting the wind turbine is either a column standing on the sea floor or a floating unit held in position by a stiff or slack mooring.

* Illustration of typical oil and gas platforms. Ormen Lange field. Offshore wind farms.

Networks of pipelines on the sea floor are important as infrastructure for oil and gas transportation. The offshore technology expertise is beneficial for novel road connections across fjords or inlets which are assumed to replace the less efficient ferry connections. The connections may be supported by a set of pontoons and may be made in the form of floating bridges or submerged floating tunnels.

* Proposed fjord connections of the coastal highway in Norway (E39).

The various constructions are exposed to forces from the ocean waves and currents. The compliant geometries, moreover, excite an ambient flow contibuting to the force picture. The forces acting on the geometry include the linear wave forces which are proportional to the wave amplitudes and oscillating with the frequencies of the wave spectrum. The excited motions of the geometry induced the added mass and damping forces. The weaker forces that are quadratic in the wave amplitudes contribute to a slowly varying drift force as well as sum frequency forces.

Other important forces acting on particularly the very slender columns supporting the offshore wind turbines include highly nonlinear forces occurring during the phase of the passing of a wave crest. They excite high frequency resonant structural motions of the geometry – termed ringing – and contribute to the fatigue of the structrure. The strongly nonlinear impact and slamming forces on ships are discussed elsewhere.

We shall include a short discussion of the velocity scaling of the huge internal waves in the sea which are capable of inducing strong bottom currents at the Ormen Lange gas field development where velocities up to 0.5 m/s have been measured at the sea floor.

An accurate evaluation of the resonance frequencies of the geometry in consideration is an important task in the wave analysis of offshore structures. In this respect the inertia force in phase with the acceleration – the added mass force – plays a fundamental role. The first task of the course is thus to develop procedures to calculate this quantity.

2 Lecture 2. Potential flow representation in an unbounded fluid. Added mass.

In this lecture the fluid flow is represented by potential theory. The fluid motion in an unbounded fluid is driven by an oscillating body in two or three dimensions. We construct a representation of the potential flow by using the singular source and dipole functions in two and three dimensions. We make use of Green's theorem and develop integral equation representation of the fluid potential. We show how to discretise and obtain by a numerical low-order collocation method the solution of the integral equations.

Using a potential flow representation, flow separation effects are disregarded. The potential flow representation is very useful when the excursions of the body are small relative to the typical diameter of the geometry. A typical situation is a body that oscillates about an equilibrium. An important effect to evaluate are the inertia forces resulting from the body motion. These are expressed in terms of a set of added mass coefficients which are evaluated from the potential flow.

2.1 Green's potential function in 2D and 3D

The Green's function solves the field equation everywhere in the fluid domain, apart from the position where the function is singular. In our cases the Green's function solves Laplace equation. In the two-dimensional case the function is $\log r$ where $r = \sqrt{(x-\bar{x})^2 + (y-\bar{y})^2}$ and $(\bar{x}, \bar{y})$ is the singular point. In three dimensions the function is $1/r$ where $r = \sqrt{(x-\bar{x})^2 + (y-\bar{y})^2 + (z-\bar{z})^2}$ and $(\bar{x}, \bar{y}, \bar{z})$ is the singular point.

2.1.1 Example

Calculate in two dimensions the volume flux at the surface $x^2 + y^2 = R_0^2$, of the source function $\log r$ where $r = \sqrt{x^2 + y^2}$. The components of the fluid velocity vector (u, v) due to the potential $\log r$ are: $u = \partial/\partial x \, \log r = (1/r)(\partial r/\partial x) = x/r^2 = x/(x^2 + y^2)$ and $v = \partial/\partial y \, \log r = (1/r)(\partial r/\partial y) = y/r^2 = y/(x^2 + y^2)$. The volume flux at the surface $r = R_0$ is $Q = \int_{r=R_0} (u, v) \cdot (n_1, n_2) dS$. The normal vector is $(n_1, n_2) = (x, y)/r$ and $dS = R_0 d\theta$ with $0 < \theta < 2\pi$. This gives $Q = 2\pi$.

2.1.2 Example

Do the same calculation in three dimensions at the surface $x^2 + y^2 + z^2 = R_0^2$, of the source function $1/r$ where $r = \sqrt{x^2 + y^2 + z^2}$. The components of the fluid velocity vector (u, v, w) due to the potential $1/r$ are: $u = \partial/\partial x \, (1/r) = -x/r^3$, $v = \partial/\partial y \, (1/r) = -y/r^3$ and $w = \partial/\partial z \, (1/r) = -z/r^3$. The volume flux at the surface $r = R_0$ is $Q = \int_{r=R_0} (u, v, w) \cdot (n_1, n_2, n_3) dS$. The normal vector is $(n_1, n_2, n_3) = (x, y, z)/r$. This gives $Q = \int_{r=R_0} (u, v, w) \cdot (n_1, n_2, n_3) dS = -(1/R_0^2) \int_{r=R_0} dS = -(1/R_0^2) \, (4\pi R_0^2) = -4\pi$.

2.2 Green's theorem

The derivations in this subsection hold both in two and three dimensions. Consider the two potential functions ϕ_1 and ϕ_2. They both satisfy the Laplace equation within a fluid

volume V bounded by the surface S which is assumed to be smooth. We have: $\nabla^2\phi_1 = 0$, $\nabla^2\phi_2 = 0$.

We investigate the combination $\nabla \cdot (\phi_1\nabla\phi_2 - \phi_2\nabla\phi_1)$. We have

$$\nabla \cdot (\phi_1\nabla\phi_2 - \phi_2\nabla\phi_1) = \nabla\phi_1 \cdot \nabla\phi_2 + \phi_1\nabla^2\phi_2 - \nabla\phi_2 \cdot \nabla\phi_1 + \phi_2\nabla^2\phi_1 = 0. \tag{1}$$

The function $\nabla\cdot(\phi_1\nabla\phi_2-\phi_2\nabla\phi_1)$ is integrated over the volume V. Using Gauss' theorem we have

$$0 = \int_V \nabla \cdot (\phi_1\nabla\phi_2 - \phi_2\nabla\phi_1)dV = \int_S \Big(\phi_1\frac{\partial\phi_2}{\partial n} - \frac{\partial\phi_1}{\partial n}\phi_2\Big)dS. \tag{2}$$

In the latter expression n denotes the unit normal along the surface S pointing out of the fluid volume where by definition $\partial/\partial n = \mathbf{n} \cdot \nabla$. The relation (2) holds in two and three dimensions where in the two-dimensional case the boundary S is replaced by a contour and the volume V is a sectional area occupied by the fluid.

2.3 Integral equation representation of the flow field in two dimensions

The relation (2) may be used to express a Laplacian potential function by a combined source and dipole distribution. It is instructive, analytically simpler and also computationally less involved to first analyse the two-dimensional case. We let $\phi_1(x, y) = \phi(x, y)$ denote the two-dimensional potential function. Further we let $\phi_2(x, y) = \log r$ where $r = \sqrt{(x - \bar{x})^2 + (y - \bar{y})^2}$. The $\log r$-function is well defined everywhere except in the singular point $(\bar{x}, \bar{y})$. In the case when $(\bar{x}, \bar{y})$ is included in the fluid volume the integration in (2) has to be modified to

$$\int_S \Big(\phi\frac{\partial}{\partial n}\log r - \frac{\partial\phi}{\partial n}\log r\Big)dS = -\int_{S_\epsilon} \Big(\phi\frac{\partial}{\partial n}\log r - \frac{\partial\phi}{\partial n}\log r\Big)dS. \tag{3}$$

The surface S_ϵ constitutes a circle of small radius ϵ that excludes a small volume surrounding the singular point $(\bar{x}, \bar{y})$ as illustrated in figure 1a. Along the contour S_ϵ the function $\partial/\partial n \log r = (1/r)\partial r/\partial n = (1/r)\mathbf{n} \cdot \nabla r = -1/r = -1/\epsilon$. The surface element along S_ϵ is parameterised by $dS = \epsilon d\theta$ where θ runs from 0 to 2π (see figure 1b). Along the integration surface S_ϵ we expand the function $\phi(x, y)$ about the point $(\bar{x}, \bar{y})$ giving $\phi(x, y) = \phi(\bar{x}, \bar{y}) + (x - \bar{x})\partial\phi/\partial x + (y - \bar{y})\partial\phi/\partial y + ... = \phi(\bar{x}, \bar{y})(1 + \mathcal{O}(\epsilon))$ where the contribution $\mathcal{O}(\epsilon) \to 0$ when $\epsilon \to 0$. Collecting the various contributions the first part of the integral on the right hand side of (3) becomes $2\pi\phi(\bar{x}, \bar{y})$. The second integral on the right hand side of (3) vanishes since $\epsilon \log \epsilon \to 0$ when $\epsilon \to 0$. In the case when $(\bar{x}, \bar{y})$ is located on the boundary S, the integration surface S_ϵ is modified to a half circle, see figure 1c, giving as result $\pi\phi(\bar{x}, \bar{y})$ for the integral on the right hand side of (3). The source function is regular in the case when $(\bar{x}, \bar{y})$ is outside of the volume V. There is no integral on the right hand side of (3). Summing up we obtain

$$\int_S \Big(\phi\frac{\partial}{\partial n}\log r - \frac{\partial\phi}{\partial n}\log r\Big)dS = \alpha\phi(\bar{x}, \bar{y}) \tag{4}$$

where $\alpha = 2\pi$ when $(\bar{x}, \bar{y})$ is in the volume V enclosed by S, $\alpha = \pi$ when $(\bar{x}, \bar{y})$ is on the boundary S and $\alpha = 0$ when $(\bar{x}, \bar{y})$ is neither in V nor on S.

When the source point is located on the fluid boundary S, equation (4) yields an integral equation to determine the potential ϕ along S, in the case when the normal derivative is given, and is obtained from the boundary value problem. When the potential along S is obtained, the same equation can be used to evaluate the potential everywhere in the fluid.

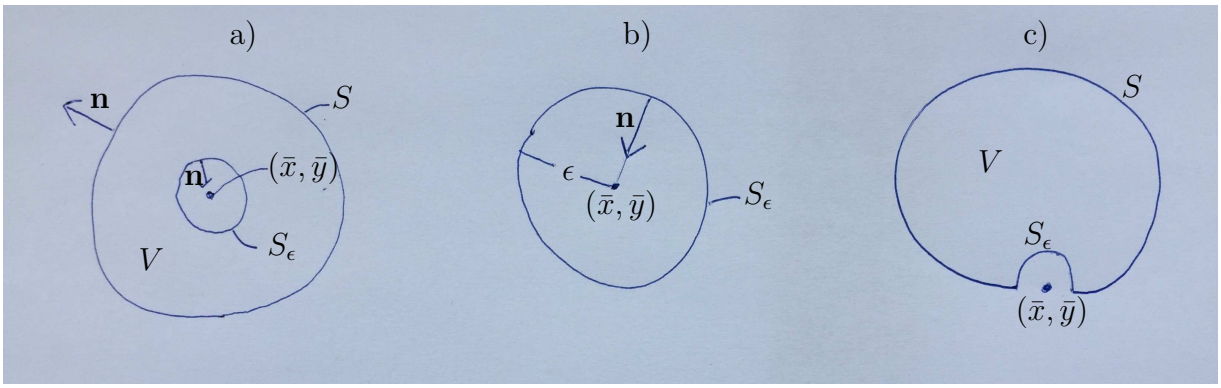

Figure 1: a) Fluid volume V bounded by a surface S and another surface S_ϵ surrounding the singular point $(\bar{x}, \bar{y})$ of the source function. The normal vector $\mathbf{n}$ of S and S_ϵ points out of the fluid. Two-dimensional case. b) The surface S_ϵ is a circle with centre in $(\bar{x}, \bar{y})$ of small radius ϵ. c) S_ϵ is a half circle when $(\bar{x}, \bar{y})$ is located on S.

2.4 Geometry moving in unbounded fluid

2.4.1 Boundary value problem in two dimensions

Consider a geometry moving with speed $U(t)$ in an unbounded fluid. The motion in the far field is at rest. We continue the analysis in two-dimensions. The corresponding three-dimensional analysis is outlined in section 2.7 below. The body geometry is represented by the surface S.

A coordinate system is fitted with the origin in the centre of the body. The x-axis is directed along the body velocity so that $\mathbf{v}_B = U(t)\mathbf{i}$. In the boundary value problem for the configuration sketched in figure 2a, the potential $\Phi(x, y, t)$ satisfies the Laplace equation in the fluid. Further the fluid velocity vanishes far away from the body giving $|\nabla\Phi| \to 0$ for $\sqrt{x^2 + y^2} \to \infty$. The kinematic boundary condition on the body reads

$$\mathbf{n} \cdot \nabla\Phi = \mathbf{n} \cdot U(t)\mathbf{i} = U(t)n_1 \quad \text{on } S, \tag{5}$$

where $\mathbf{n} = (n_1, n_2)$. The boundary value problem for Φ is reformulated by putting

$$\Phi(x, y, t) = U(t)\phi(x, y), \tag{6}$$

where $\phi(x, y)$ is independent of time and satisfies

$$\nabla^2\phi = 0 \quad \text{in } V, \tag{7}$$

$$|\nabla\phi| \to 0 \quad \sqrt{x^2+y^2} \to \infty, \tag{8}$$

$$\frac{\partial\phi}{\partial n} = n_1 \quad \text{on } S. \tag{9}$$

The solution of the boundary value problem (7)-(9) is expressed in terms of an integral equation similar to (4) where now the fluid domain is exterior to the geometry. The fluid volume is also bounded by a control surface at distant radius where the contribution vanishes because the fluid motion has a fast decay in the far distance. While the potential ϕ is unknown, both in the fluid volume and on the boundary S as well, the kinematic boundary condition on S given by (9) determines $\partial\phi/\partial n$. In the case when $(\bar{x},\bar{y})$ is on S the velocity potential is obtained formally by

$$-\pi\phi(\bar{x},\bar{y}) + \int_S \phi\frac{\partial}{\partial n}\log r\, dS = \int_S \frac{\partial\phi}{\partial n}\log r\, dS, \tag{10}$$

where $\partial\phi/\partial n = n_1$ along S. A numerical solution of (10) for a geometry of arbitrary shape is discussed in section 2.6 below.

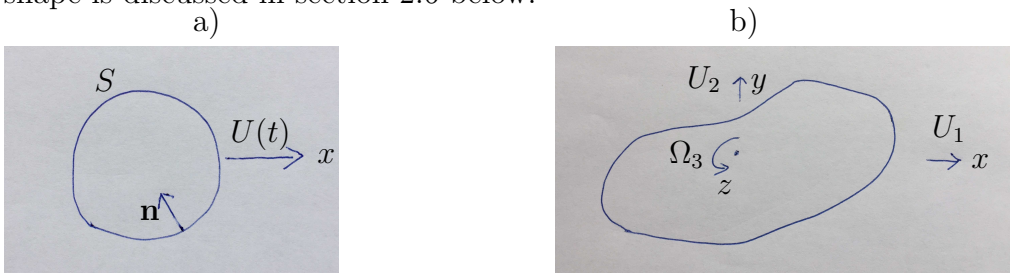

Figure 2: a) Two-dimensional geometry with a) speed $U(t)$ along the x-axis. Normal vector $\mathbf{n}$ along the boundary S points out of the fluid (into the geometry); b) speed $U_1(t)$ along the x-axis, $U_2(t)$ along the y-axis and angular velocity $\Omega_3(t)$ along the z-axis (pointing out of the two-dimensional plane).

2.5 Force on the geometry

Having formally obtained the flow potential by the integral equation (10) – which we solve numerically in section 2.6 below, the pressure p in the fluid is obtained from the Bernoulli equation giving

$$p = -\rho\Big(\frac{\partial\Phi}{\partial t} + \frac{1}{2}|\nabla\Phi|^2\Big) \simeq -\rho\frac{\partial\Phi}{\partial t} = -\rho\dot{U}\phi(x,y). \tag{11}$$

In (11) the leading contribution of the pressure – the linear acceleration term – is retained, where $\dot{U} = dU/dt$. The linearisation in (11) is valid for small oscillations of the geometry which is assumed here. The force on the two-dimensional geometry is obtained by

$$F_1 = \int_S pn_1 dS \simeq -\rho\dot{U}\int_S \phi n_1 dS, \tag{12}$$

$$F_2 = \int_S pn_2 dS \simeq -\rho\dot{U}\int_S \phi n_2 dS, \tag{13}$$

where (F_1, F_2) denotes the force vector and the normal vector is expressed by (n_1, n_2). The moment with respect to the z-axis directed along the $\mathbf{k} = \mathbf{i} \times \mathbf{j}$ vector is expressed by

$$M_3 = \int_S p n_6 dS \simeq -\rho \dot{U} \int_S \phi n_6 dS, \tag{14}$$

where $n_6 = x n_2 - y n_1$. For convenience we denote $M_3 = F_6$. The relations (12)-(14) give

$$F_i = -\dot{U} m_{1i}, \quad m_{1i} = \rho \int_S \phi n_i dS, \quad i = 1, 2, 6, \tag{15}$$

where (15) expresses the force components and moment in terms of the added mass coefficients m_{1i} $(i = 1, 2, 6)$ times the acceleration $\dot{U}$ of the body along the x-direction. The components n_i of the generalized normal vector are defined below (13) and (14).

The two-dimensional geometry may generally translate with a speed $U_1(t)$ along the x-axis, $U_2(t)$ along the y-axis and rotate with an angular velocity $\Omega_3(t)$ about the z-axis, see figure 2b. It is convenient to write $\Omega_3 = U_6$. The velocity potential is conveniently decomposed by

$$\Phi(x, y, t) = U_1(t)\phi_1(x, y) + U_2(t)\phi_2(x, y) + U_6(t)\phi_6(x, y) \tag{16}$$

where the potentials $\phi_i(x, y)$ $(i = 1, 2, 6)$ are independent of time. The potentials satisfy the Laplace equation in the fluid domain, $|\nabla \phi_i| \to 0$ in the far field, and

$$\frac{\partial \phi_i}{\partial n} = n_i \quad \text{on } S, \quad i = 1, 2, 6. \tag{17}$$

The components of the linear pressure force are obtained similarly as in (15) by

$$F_i = -\sum_j \dot{U}_j m_{ji} \quad \text{where} \quad m_{ji} = \rho \int_S \phi_j n_i dS, \tag{18}$$

where m_{ji} denotes the added mass matrix for a two-dimensional geometry and the sum in (18) is over $j = 1, 2, 6$.

2.5.1 Example. Added mass of a circular cross-section

The potential ϕ_1 for a circular cylinder section of radius R_0 performing a translation in the x-direction is given by the two-dimensional dipole by

$$\phi_1 = -R_0^2 \frac{\partial}{\partial x} \log \sqrt{x^2 + y^2} = -\frac{R_0^2 x}{x^2 + y^2}. \tag{19}$$

The x-component of the normal vector along the boundary S at $x^2 + y^2 = R_0^2$ is $n_1 = -x/\sqrt{x^2 + y^2}$, and a parameterisation of S gives $dS = R_0 d\theta$ with $0 < \theta < 2\pi$. The added mass coefficient m_{11} becomes

$$m_{11} = \rho \int_S \phi_1 n_1 dS = \rho \int_0^{2\pi} \frac{-R_0^2 x}{x^2 + y^2} \frac{-x}{\sqrt{x^2 + y^2}} R_0 d\theta = \rho R_0^2 \int_0^{2\pi} \cos^2\theta d\theta = \rho \pi R_0^2 = \rho \mathcal{A}, \tag{20}$$

and shows that m_{11} corresponds to the displaced mass of the sectional area $\mathcal{A}$ of the circle.

2.6 Integral equation on discrete form

There are several ways to obtain a numerical solution of (10). A straightforward method which obtains a satisfactory convergence is to discretise the surface S by a number of segments S_j and assume that the potential and its normal derivative are constant on each segment. A discrete version of (10) becomes

$$-\pi\phi(\bar{x},\bar{y}) + \sum_{m=1}^{N} \phi_m \int_{S_m} \frac{\partial}{\partial n} \log r dS = \sum_{m=1}^{N} \Big[\frac{\partial \phi}{\partial n}\Big]_m \int_{S_m} \log r dS. \tag{21}$$

Each segment S_m is approximated by a straight line specified by its end points (x_{m-1}, y_{m-1}) and (x_m, y_m) where figure 3a illustrates a subdivision with 8 segments. The discrete equation (21) may be satisfied in the centroid of each segment S_n at $(\bar{x}_n, \bar{y}_n) = (\frac{1}{2}(x_{n-1} + x_i), \frac{1}{2}(y_{n-1} + y_n))$.

Evaluating the flux integral $\int_{S_m}(\partial/\partial n)\log r dS$ we use that $n_1 dS = -dy$ and $n_2 dS = dx$ where (n_1, n_2) is the normal vector on segment S_m, pointing out of the fluid, giving

$$\begin{aligned}\int_{S_m} \frac{\partial}{\partial n} \log r dS &= \int_{S_m} n_1 \frac{\partial}{\partial x} \log r dS + n_2 \frac{\partial}{\partial y} \log r dS \\ &= \int_{S_m} \Big(\frac{\partial}{\partial x} \log r(-dy) + \frac{\partial}{\partial y} \log r(dx) \Big)\end{aligned} \tag{22}$$

Introducing the complex variable $z = x + \mathrm{i}y$ where i is the imaginary unit we obtain for the integral

$$\begin{aligned}\int_{S_m} \frac{\partial}{\partial n} \log r dS &= \int_{S_m} Re\Big(\frac{\partial}{\partial x} \log(z - \bar{z}_n)(-dy) + \frac{\partial}{\partial y} \log(z - \bar{z}_n)(dx) \Big) \\ &= -\int_{S_m} Im\Big(\frac{dz}{z - \bar{z}_n} \Big) = -\int_{S_m} Im \log(z - \bar{z}_n)|_{z_{m-1}}^{z_m} = -\Delta\Theta_{n,m},\end{aligned} \tag{23}$$

where Re denotes real part and Im imaginary part. Eq. (23) shows that the flux integral $\int_{S_m}(\partial/\partial n)\log r dS = -\Delta\Theta_{n,m}$ equals the negative of the opening angle defined by the segment S_m due to a source in the collocation point $(\bar{x}_n, \bar{y}_n)$. The minus sign is caused by the normal pointing into the geometry (figure 2a). In the case when $(\bar{x}_n, \bar{y}_n)$ is on S_m $(n = m)$ the flux integral for the straight segment is zero.

The integral $\int_{S_m} \log r dS$ on the right hand side of (21) may be evaluated quite accurately by use of two-points Gauss integration giving

$$\begin{aligned}h_{n,m} &= \int_{S_m} \log r dS \\ &\simeq \tfrac{1}{2}[\log((x_m^{(1)} - \bar{x}_n)^2 + (y_m^{(1)} - \bar{y}_n)^2) + \log((x_m^{(2)} - \bar{x}_n)^2 + (y_m^{(2)} - \bar{y}_n)^2)](\tfrac{1}{2}\Delta S_m)\end{aligned} \tag{24}$$

where ΔS_m is the length of segment S_m and the evaluation points $(x_m^{(1,2)}, y_m^{(1,2)})$ of the two-points Gauss integration are given by

$$x_m^{(1,2)} = \pm\tfrac{1}{2}(x_m - x_{m-1})\tfrac{\sqrt{3}}{3} + \tfrac{1}{2}(x_{m-1} + x_m), \quad y_m^{(1,2)} = \pm\tfrac{1}{2}(y_m - y_{m-1})\tfrac{\sqrt{3}}{3} + \tfrac{1}{2}(y_{m-1} + y_m). \tag{25}$$

The resulting integral equation on discrete form becomes

$$-\pi\phi_n + \sum_{m=1}^{N} \phi_m(-\Delta\Theta_{n,m}) = \sum_{m=1}^{N} \left[\frac{\partial\phi}{\partial n}\right]_m h_{n,m}, \quad n = 1, 2, ..N \tag{26}$$

obtaining ϕ_n on each segment. The normal derivative $[\partial\phi/\partial n]_m$ is specified for each of the potentials where $\partial\phi_i/\partial n = n_i$ for $i = 1, 2, 6$ in two dimensions where n_i is the generalized normal vector on the segment S_m evaluated in the position $\bar{x}_m = \frac{1}{2}(x_{m-1}+x_m)$, $\bar{y}_m = \frac{1}{2}(y_{m-1} + y_m)$.

The added mass coefficients may be calculated by the approximation

$$m_{ji} = \rho \int_S \phi_j n_i dS \simeq \rho \sum_{m=1}^{N} [\phi_j]_m [n_i]_m \Delta S_m. \tag{27}$$

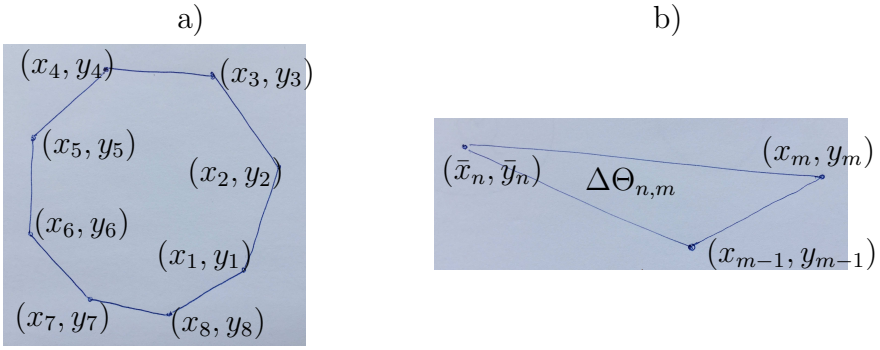

Figure 3: a) Geometry S discretised by a number of $N = 8$ segments S_m, each stretching between the coordinates (x_{m-1}, y_{m-1}) and (x_m, y_m). b) Opening angle $\Delta\Theta_{n,m}$ of segment S_m defined from the source point $(\bar{x}_n, \bar{y}_n)$.

2.6.1 Exercises

1. Make discretisations of a) a circle with radius R_0, b) and ellipse of major half axis a_0 and minor half axis b_0, and c) a square of side $2a_0$. Use a Matlab or Python-script for the purpose.

2. Calculate the coefficients of the integral equation on discrete form (26). Solve the integral equation for the circle and compare to the analytical solution in (19). Investigate convergence as function of N (hint: use $N = 100$, 200 and 400.)

3. Calculate the added mass coefficient a_{11} of the circle. Compare to the analytical result $m_{11} = \rho\,\pi R_0^2$.

4. Do the same for the ellipse with $b_0/a_0 = 0.5$ and $b_0/a_0 = 0.1$. Solve the discrete integral equation (26). Investigate convergence as function of the number of segments N. Calculate the added mass coefficients for the ellipse and compare to the exact results: $m_{11} = \rho\,\pi b_0^2$, $m_{22} = \rho\,\pi a_0^2$, $m_{66} = (1/8)\rho\,\pi(a_0^2 - b_0^2)^2$,

5. Do the same for the square. Solve the discrete integral equation (26). Investigate convergence. Calculate the added mass coefficients and compare to the exact results: $m_{11}/\rho = 4.754a_0^2$, $m_{22}/\rho = 4.754a_0^2$, $m_{66}\rho = 0.725a_0^4$.

2.6.2 MATLAB calculation of the potential and added mass of a circle

Below is a MATLAB script that calculates the potential and added mass of a circle, see the exercise given in section 2.6.1.

```
%N=20; %N=40;
N=80;
thetap=linspace(2*pi/N,2*pi,N);
thetam=linspace(0,2*pi*(N-1)/N,N);
xp=cos(thetap);
yp=sin(thetap);
xm=cos(thetam);
ym=sin(thetam);
barx=0.5*(xp+xm);
bary=0.5*(yp+ym);
ds=((xp-xm).^2+(yp-ym).^2).^(1/2);
nn1=-barx./(barx.^2+bary.^2).^(1/2);
for i=1:N;
hh(i)=0.0;
help=0.0;
for j=1:N;
a1=xm(j)-barx(i);
a2=ym(j)-bary(i);
b1=xp(j)-barx(i);
b2=yp(j)-bary(i);
arg=acos((a1*b1+a2*b2)/sqrt((a1^2+a2^2)*(b1^2+b2.^2)));
dtheta(i,j)=-arg;
if j-i == 0
   dtheta(i,j)=-pi;
end
x1g=0.5*(xp(j)-xm(j))/sqrt(3)+barx(j);
y1g=0.5*(yp(j)-ym(j))/sqrt(3)+bary(j);
x2g=-0.5*(xp(j)-xm(j))/sqrt(3)+barx(j);
y2g=-0.5*(yp(j)-ym(j))/sqrt(3)+bary(j);
hh0=log((x1g-barx(i))^2+(y1g-bary(i))^2);
hh0=hh0+log((x2g-barx(i))^2+(y2g-bary(i))^2);
hh0=hh0*0.5;
help=help+hh0*nn1(j)*ds(j)/2;
end
hh(i)=help;
end
pdcr=dtheta\hh';
pan=-barx./(barx.^2+bary.^2);
hold on
axis ([0 2*pi -1.1 1.1])
g0=plot(0.5*(thetap+thetam),pdcr,'k .');
```

```
plot(0.5*(thetap+thetam),pan,'k -');
get(g0)
set(g0,'MarkerSize',[8])
set(gca,'FontSize',20)
da11=pdcr'.*nn1.*ds;
a11=sum(da11)/pi
```

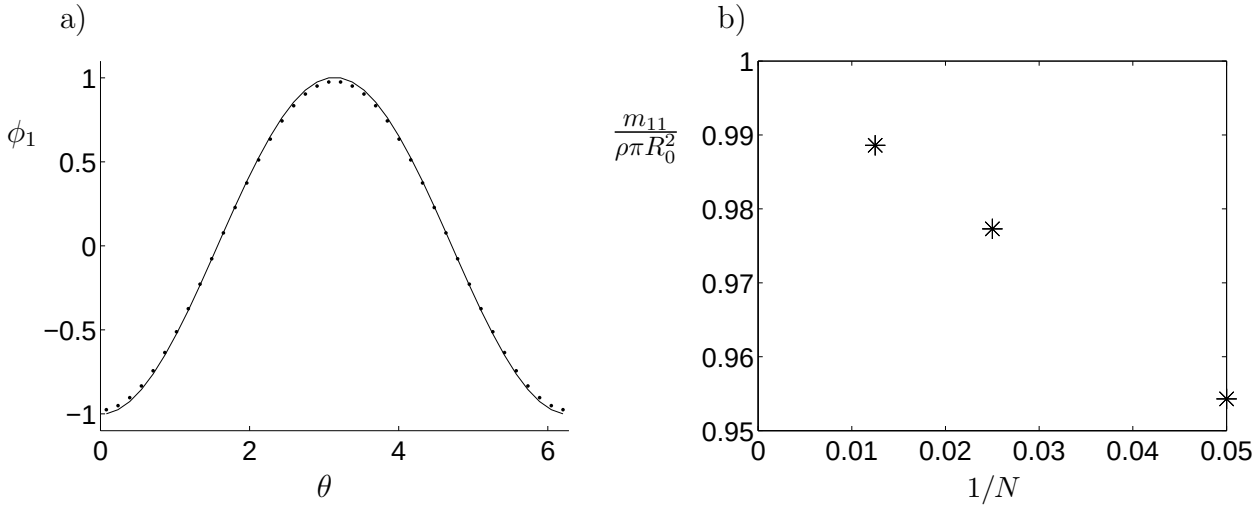

Figure 4: a) Potential ϕ_1 along a circle discretised by $N = 40$ points (symbols) compared to the analytical potential eq. (19) as function of $\theta = \arccos(x/R_0)$ with $R_0 = 1$. b) Computed added mass m_{11} of the circle divided by the analytical added mass $\rho\pi R_0^2$ as function of the inverse of the resolution.

Figure 4a,b shows the computed potential ϕ_1 for a circle in lateral motion with resolutions of $N = 40$ and $N = 80$, with comparison to the analytical solution in eq. (19). The numerical solution converges to the analytical solution as N increases.

The calculated added mass coefficient divided by the analytical one corresponding to $m_{11}/\rho\pi R_0^2$ shows that the ratio is 0.9543 ($N = 20$), 0.9773 ($N = 40$) and 0.9886 ($N = 80$). and converges towards 1 as $1/N$ tends to zero (figure 4c).

2.7 Generalisation to three dimensions

The motion of a body in three dimensions has six degrees of freedom, where three are in translation and three in rotation. Let (U_1, U_2, U_3) denote the instantaneous translatory velocity and $(\Omega_1, \Omega_2, \Omega_3)$ the instantaneous angular velocity of the geometry. The velocity at a position (x, y, z) on the body is expressed by

$$\mathbf{v}_P = (U_1, U_2, U_3) + (\Omega_1, \Omega_2, \Omega_3) \times (x, y, z), \tag{28}$$

and is exact. For convenience we write $U_j = \Omega_{j-3}$, $j = 4, 5, 6$. The Laplacian velocity potential due to the body is similarly as in two dimensions decomposed by

$$\Phi(x, y, z, t) = \sum_{j=1}^{6} U_j \phi_j(x, y, z) \tag{29}$$

where ϕ_j satisfy the Laplace equation in the fluid and $|\nabla\phi| \to 0$ for $\sqrt{x^2+y^2+z^2} \to \infty$. The kinematic boundary condition at the body, i.e. $\mathbf{n} \cdot \mathbf{v}_P = \mathbf{n} \cdot \nabla\Phi$, gives that

$$\frac{\partial \phi_j}{\partial n} = n_j \quad j = 1, 2, ...6, \tag{30}$$

where $(n_1, n_2, n_3) = \mathbf{n}$ denotes the unit normal vector along the surface S of the body in the three-dimensional case and $(n_4, n_5, n_6) = \mathbf{x} \times \mathbf{n}$ defines the components n_j, $j = 4, 5, 6$.

Solution of the boundary value problems for ϕ_j in the three-dimensional case are expressed in terms of a set of integral equations similarly as in two dimensions, where the function $\log r$ is replaced by the three-dimensional source function $1/|(x, y, z) - (\bar{x}, \bar{y}, \bar{z})|$. It may be shown that

$$\int_S \Big(\phi \frac{\partial}{\partial n}\frac{1}{r} - \frac{\partial \phi}{\partial n}\frac{1}{r}\Big) dS = -\alpha\phi(\bar{x}, \bar{y}, \bar{z}) \tag{31}$$

where $\alpha = 4\pi$ for $(\bar{x}, \bar{y}, \bar{z})$ in the fluid volume, $\alpha = 2\pi$ for $(\bar{x}, \bar{y}, \bar{z})$ on the boundary S and $\alpha = 0$ for $(\bar{x}, \bar{y}, \bar{z})$ neither in V nor on S.

The components of the force vector (F_1, F_2, F_3) and moment (M_1, M_2, M_3) are expressed by the accelerations $\dot{U}_i$ by

$$F_j = -\sum_{i=1}^{6} \dot{U}_i m_{ji}, \quad \text{where} \quad m_{ji} = \rho \int_S \phi_i n_j dS \tag{32}$$

where m_{ji} denote the six by six added mass matrix and $F_j = M_{j-3}$ for $j = 4, 5, 6$.

2.7.1 Symmetry of the added mass matrix

From the kinematic boundary condition (30) we have that $n_j = \partial\phi_j/\partial n$. This means that the added mass matrix may alternatively be written by $m_{ji} = \rho \int_S \phi_i(\partial\phi_j/\partial n)dS$. By use of Green's theorem (2) in three dimensions we obtain

$$m_{ji} - m_{ij} = \rho \int_S \Big(\phi_i \frac{\partial \phi_j}{\partial n} - \phi_j \frac{\partial \phi_i}{\partial n}\Big) dS = 0, \tag{33}$$

and shows that the added mass matrix is symmetric where $m_{ji} = m_{ij}$.

2.7.2 Kinetic energy of the fluid expressed by the added mass matrix

The added mass matrix has another property in that it expresses the kinetic energy of the fluid motion. The kinetic energy of the fluid motion in the volume V is expressed by

$$\begin{aligned} T &= \frac{1}{2}\int_V \rho \nabla\Phi \cdot \nabla\Phi dV = \frac{\rho}{2}\int_V \nabla \cdot (\Phi\nabla\Phi) dV = \frac{\rho}{2}\int_S \Phi \frac{\partial \Phi}{\partial n} dS \\ &= \frac{1}{2}\sum_{i,j=1}^{6} U_i U_j \rho \int_S \phi_i \frac{\partial \phi_j}{\partial n} dS = \frac{1}{2}\sum_{i,j=1}^{6} U_i U_j m_{ij}, \end{aligned} \tag{34}$$

where Gauss' theorem and the definition (29) have been used.

2.7.3 Example. Added mass of a sphere

The potential ϕ_1 for a sphere of radius R_0 translating along the x-direction is given by

$$\phi_1 = \frac{R_0^3}{2}\frac{\partial}{\partial x}\frac{1}{r} = -\frac{R_0^3 x}{2r^3}, \tag{35}$$

where $r = \sqrt{x^2+y^2+z^2}$. Further, $n_1 = -x/r$ at $r = R_0$. The added mass m_{11} is obtained by integrating the product $\phi_1 n_1$ over the surface of the sphere. Multiplying by the density we obtain

$$m_{11} = \rho \int_S \frac{(-R_0^3 x)}{2r^3}\frac{(-x)}{r} dS = \frac{\rho}{2R_0}\int_S x^2 dS = \frac{\rho}{2}\frac{4\pi R_0^3}{3} = \frac{1}{2}\rho\mathcal{V}, \tag{36}$$

and shows that m_{11} corresponds to half of the displaced mass of the sphere of volume $\mathcal{V}$. In (36) we have used that $\int_S x^2 dS = \int_S y^2 dS = \int_S z^2 dS = (1/3)R_0^2 \int_S dS = (4\pi/3)R_0^4$.

3 Lecture on: The force and moment on a geometry moving in and unbounded fluid.

We shall obtain the force and moment on a rigid body moving in unbounded fluid. The body is defined by its surface S_B and its rigid body-motion, where the velocity is given by $\mathbf{v}_B$ at any point along S_B. A geometrical surface S_C completely surrounds the body. Balance of momentum of the fluid occupied by the volume V, enclosed by S_B and S_C reads

$$\rho\frac{\partial \mathbf{v}}{\partial t} + \rho\nabla\cdot(\mathbf{v}\mathbf{v}) + \nabla p = 0, \tag{37}$$

where $\mathbf{v}$ denotes the fluid velocity, p the pressure and ρ the constant density of the fluid. We assume that the fluid velocity is expressed by the velocity potential ϕ where $\mathbf{v} = \nabla\phi$. In (37) we have assumed that the fluid is incompressible with $\nabla\cdot\mathbf{v} = 0$ giving that the convective term of the equation of motion may be written by $\mathbf{v}\cdot\nabla\mathbf{v} = \nabla\cdot(\mathbf{v}\mathbf{v})$. Integrating (37) over the volume V obtains

$$\rho\int_V \frac{\partial \mathbf{v}}{\partial t}dV + \rho\int_V \nabla\cdot(\mathbf{v}\mathbf{v})dV + \int_V \nabla p dV = 0 \tag{38}$$

By use of Gauss' theorem, terms 2 and 3 in (38) are rewritten by

$$\rho\int_V \nabla\cdot(\mathbf{v}\mathbf{v})dV = \rho\int_{S_B}\mathbf{v}v_n dS + \rho\int_{S_C}\mathbf{v}v_n dS, \tag{39}$$

$$\int_V \nabla p dV = \int_{S_B} p\mathbf{n}dS + \int_{S_C} p\mathbf{n}dS, \tag{40}$$

where $\mathbf{n}$ denotes the unit normal pointing out of the fluid (into the body), $v_n = \mathbf{v}\cdot\mathbf{n}$, and where $\int_{S_B} p\mathbf{n}dS = \mathbf{F}$ gives the pressure force on S_B. By use of the transport theorem we derive a modified relation involving term 1 in (38)

$$\rho\frac{d}{dt}\int_V \mathbf{v}dV = \rho\int_V \frac{\partial \mathbf{v}}{\partial t}dV + \rho\int_{S_B}\mathbf{v}\mathbf{v}_B\cdot\mathbf{n}dS, \tag{41}$$

where $\mathbf{v}_B\cdot\mathbf{n}$ is the normal velocity of the surface S_B. Note that $\mathbf{v}_B\cdot\mathbf{n} = \mathbf{v}\cdot\mathbf{n} = v_n$ on S_B. The term on the left hand side of (41) is further developed by use of Gauss' theorem:

$$\rho\frac{d}{dt}\int_V \mathbf{v}dV = \rho\frac{d}{dt}\int_{S_B}\phi\mathbf{n}dS + \rho\frac{d}{dt}\int_{S_C}\phi\mathbf{n}dS = \rho\frac{d}{dt}\int_{S_B}\phi\mathbf{n}dS + \rho\int_{S_C}\frac{\partial\phi}{\partial t}\mathbf{n}dS \tag{42}$$

where the time integration may be taken inside the integral over S_C since this surface is geometrical. Combination of (38)–(42) gives

$$\rho\frac{d}{dt}\int_{S_B}\phi\mathbf{n}dS + \int_{S_C}\Big[\Big(p+\rho\frac{\partial\phi}{\partial t}\Big)\mathbf{n} + \rho\mathbf{v}v_n\Big]dS + \mathbf{F} = 0. \tag{43}$$

The pressure along the control surface S_c is given by the Bernoulli equation by $p+\rho\partial\phi/\partial t+(1/2)\rho\mathbf{v}^2+C(t) = 0$ where the constant $C(t)$ gives no contribution over the closed surface S_c. From (43) we obtain

$$\mathbf{F} = -\rho\frac{d}{dt}\int_{S_B}\phi\mathbf{n}dS - \rho\int_{S_C}\Big(\mathbf{v}v_n - \frac{1}{2}\mathbf{v}^2\mathbf{n}\Big)dS. \tag{44}$$

The similar relation may be derived for the moment of the pressure forces on the body obtaining

$$\mathbf{M} = -\rho \frac{d}{dt} \int_{S_B} \phi \mathbf{r} \times \mathbf{n} dS - \rho \int_{S_C} \mathbf{r} \times \Big(\mathbf{v} v_n - \frac{1}{2} \mathbf{v}^2 \mathbf{n} \Big) dS. \tag{45}$$

In (44)–(45) $\mathbf{v} = \nabla \phi$ and $v_n = \partial \phi / \partial n$. In (45) the vector $\mathbf{r}$ denotes the moment arm. In the derivation of (45) we have used

$$\int_V \mathbf{r} \times \nabla(\ ) dV = - \int_V \nabla \times \Big(\mathbf{r}(\ ) \Big) dV, \tag{46}$$

which holds, since $\nabla \times \mathbf{r} = 0$. Use of a variant of Stokes theorem gives

$$- \int_V \nabla \times \Big(\mathbf{r}(\ ) \Big) dV = - \int_{S_B + S_C} \mathbf{n} \times \Big(\mathbf{r}(\ ) \Big) dS = \int_{S_B + S_C} \mathbf{r} \times \Big(\mathbf{n}(\ ) \Big) dS, \tag{47}$$

and (45) follows.

4 Water waves in deep water. Key properties

UNFINISHED

4.1 Key subjects

* Unidirectional, monochromatic gravity waves in deep water

* Linear kinematic and dynamic free surface boundary condition

* Wavenumber, wavelength, wave frequency, period

* Wave amplitude and waveslope

* Dispersion relation

* Group velocity

* Mean energy flux

* Mean energy density

4.2 The motion of deep water waves

We introduce the horizontal coordinate x directed along the wave propagation direction. The waves propagate along the surface of a fluid where the surface at rest is located at $y = 0$. The motion is driven by gravity where g denotes the acceleration of gravity. The fluid is assumed to be incompressible and inviscid. The wave propagation is governed by the Laplacian potential Φ.

The kinematic boundary condition at the free surface reads

$$\frac{D}{Dt}(y - \eta) = 0 \quad \text{on} \quad y = \eta, \tag{48}$$

where the surface elevation is function of x and t (time) with $\eta(x, t)$. The material derivative reads $D/Dt = \partial/\partial t + \nabla\Phi \cdot \nabla$. The dynamic boundary condition at the free surface reads

$$p = p_0 \quad \text{on} \quad y = \eta, \tag{49}$$

and expresses that the fluid pressure at the surface equals the constant pressure above the surface. The fluid pressure is obtained from the Bernoulli equation which reads $p/\rho = -\partial\Phi/\partial t - \frac{1}{2}|\nabla\Phi|^2 - gy + p_0/\rho$.

We shall consider linear wave motion where the conditions (48) and (49) are linearized, giving

$$\frac{\partial\Phi}{\partial y} - \frac{\partial\eta}{\partial t} = 0, \quad \frac{\partial\Phi}{\partial t} + g\eta = 0 \quad \text{on} \quad y = 0. \tag{50}$$

The kinematic and dynamic conditions in (50) may be combined giving

$$\frac{\partial^2\Phi}{\partial t^2} + g\frac{\partial\Phi}{\partial y} = 0, \quad \frac{\partial\Phi}{\partial t} + g\eta = 0 \quad \text{on} \quad y = 0. \tag{51}$$

The wave motion has to decay in the deep water which means that $|\nabla\Phi \to 0|$ for $y \to -\infty$.

We shall assume that the wave motion is periodic with the wave frequency ω. The wave potential is conveniently written by $\Phi(x,y,t) = Re[\phi(x,y)e^{\mathrm{i}\omega t}]$ where $\phi(x,y)$ is also Laplacian. The free surface boundary condition (51) becomes, for the period motion

$$-\omega^2\phi + g\frac{\partial\phi}{\partial y} = 0 \quad \text{on} \quad y = 0. \tag{52}$$

A wave propagation along the positive x-axis implies that $\phi(x,y) = f_0(y)e^{-\mathrm{i}kx}$. Since ϕ is Laplacian the vertical dependency is $f_0(y) = C\,e^{ky}$ where $f_0 \to 0$ for $y \to -\infty$ and C is a constant.

The wave elevation is obtained from the second equation in (50) which gives

$$\eta = -\frac{1}{g}\frac{\partial\Phi}{\partial t} = Re\Big((-\mathrm{i}C/g)e^{\mathrm{i}(\omega t - kx)}\Big) = A\cos(\omega t - kx), \tag{53}$$

where $y = 0$ is inserted in $f_0(y)$. In (53) the quantity A is referred to as the wave amplitude and k is the wavenumber. The coefficient C is related to the amplitude by $C = \mathrm{i}gA/\omega$. The wave potential thus becomes

$$\Phi(x,y,t) = Re\Big(\phi(x,y)e^{\mathrm{i}\omega t}\Big), \quad \phi(x,y,t) = \frac{\mathrm{i}gA}{\omega}e^{ky-\mathrm{i}kx} \tag{54}$$

4.2.1 Dispersion relation

We are now using the linear free surface boundary condition. The potential (54) is inserted into (52), giving

$$\omega^2 = gk, \tag{55}$$

and expresses the linear dispersion relation for gravity waves in deep water.

4.2.2 Propagation speed, period and wavelength

The wave crests (or troughs) propagate with constant phase where

$$kx - \omega t = k\Big(x - \frac{\omega}{k}t\Big) = const. \tag{56}$$

This defines the wave propagation speed c of deep water waves where

$$c = \frac{\omega}{k} = \frac{g}{\omega} = \sqrt{\frac{g}{k}}, \tag{57}$$

and demonstrates that longer deep water gravity waves (smaller k) move faster than shorter waves.

Wave period T and wavelength λ are defined by

$$T = \frac{2\pi}{\omega}, \quad \lambda = \frac{2\pi}{k}. \tag{58}$$

4.3 Energy density

Consider a volume V in the form of a vertical slice of the wave motion bounded by the vertical planes at positions x and $x + \Delta x$ and above by the surface $y = \eta$. The volume extends a unit length laterally.

The time averaged kinetic energy in this volume is given by the integral

$$\Delta E_K = \overline{\int_V \tfrac{1}{2}\rho(u^2 + v^2)dy}\Delta x \tag{59}$$

where $(u, v) = \nabla\Phi$ and an overline denotes time average. With the potential Φ given in (54) we have

$$u^2 = A^2\omega^2 e^{2ky}\cos^2(kx - \omega t), \quad v^2 = A^2\omega^2 e^{2ky}\sin^2(kx - \omega t), \quad u^2 + v^2 = A^2\omega^2 e^{2ky}. \tag{60}$$

The time averaged kinetic energy per Δx – the mean kinetic energy density – is obtained by

$$\Delta E_K/\Delta x = \overline{\tfrac{1}{2}\rho A^2\omega^2 \textstyle\int_{-\infty}^{0} e^{2ky}dy} = \tfrac{1}{4}\rho g A^2(1 + O(A^2)) \tag{61}$$

where $\omega^2 = gk$ has been used.

The time averaged excess potential energy is given by

$$\Delta E_P = \Delta x \overline{\int_0^\eta \rho g y dy} = \Delta x\ \tfrac{1}{2}\rho g\overline{\eta^2} \tag{62}$$

giving that the excess potential energy per Δx and averaged in time becomes $\frac{1}{4}\rho g A^2$. The sum $\Delta E_K/\Delta x + \Delta E_P/\Delta x$ averaged in time becomes

$$\bar{E} = \tfrac{1}{2}\rho g A^2 \tag{63}$$

and defines the mean energy density per unit crest length of gravity waves in deep water.

4.4 Group velocity

The group velocity is defined by (mathematical illustration to be added)

$$c_g = \frac{\partial\omega}{\partial k}. \tag{64}$$

The group velocity of deep water waves with $\omega^2 = gk$ becomes $\partial\omega/\partial k = \frac{1}{2}(\omega/k) = \frac{1}{2}c$.

4.5 Energy flux

The energy flux at a surface S is defined by $Energy\,Flux = \int_S (p + \frac{1}{2}\rho\mathbf{v}^2 + \rho g y)\mathbf{v}\cdot\mathbf{n}dS$. We evaluate the time averaged energy flux of the wave motion at a surface $x = const.$ obtaining

$$\overline{Energy\,Flux} = \overline{\int_{-\infty}^{\eta} -\rho\frac{\partial\Phi}{\partial t}\frac{\partial\Phi}{\partial x}dy.} = \int_{-\infty}^{0} -\rho\overline{\frac{\partial\Phi}{\partial t}\frac{\partial\Phi}{\partial x}}dy(1 + O(A^2)). \tag{65}$$

Inserting the wave potential Φ given in (54) we obtain, taking into account the leading terms,

$$\overline{Energy\,Flux} = \int_{-\infty}^{0} \rho g A^2 \omega e^{2ky} \overline{\cos^2(kx - \omega t)} dy = \tfrac{1}{4} \rho g A^2 \omega / k = \bar{E}\ \partial\omega/\partial k \qquad (66)$$

and expresses that the time averaged energy flux at a control surface $x = const.$ is the energy density of the wave times the group velocity.

5 Wave analysis of a floating geometry in two dimensions

5.1 Contents

5.2 Discretisation of the geometry
5.3 The wave Green function in two dimensions
5.4 Test of the integral equation in the diffraction problem
5.5 Discretisation of the integral equation
5.6 The radiation problem
5.6.1 Obtaining the damping force from the far field energy flux
5.6.2 Numerical solution of the integral equation
5.7 The diffraction problem
5.7.1 Integral equation in the diffraction problem
5.7.2 The exciting force
5.7.3 Haskind relations
5.7.4 Approximations of the exciting force
5.8 Response in heave. Resonance
5.8.1 Approximate analysis of a narrow box section
5.9 Calculation of the response in a realistic sea state

5.2 Discretisation of the geometry

The task starts by making a geometry. Each segment S_m of the wetted body surface S_B are defined by the start and end points, (xm(i),ym(i)) and (plus) (xp(i),yp(i)), respectively, organised as coord2=[xm(i),ym(i),xp(i),yp(i)] with output in the ascii-file box.dat:

```
xm(1),ym(1),xp(1),yp(1)
xm(2),ym(2),xp(2),yp(2)
xm(3),ym(3),xp(3),yp(3)
.
.
```

```
% box of draught D and length (width) L, with D as unit length
% left vertical side
D=1;
L=2;
Nside=10;
Nbott=20;
N=Nside+Nbott+Nside;
dy=D/Nside;
dx=L/Nbott;
xp(1)=-L/2;
xm(1)=-L/2;
yp(1)=-dy;
ym(1)=-dy*(1-1);
```

```
coord=[xm(1),ym(1),xp(1),yp(1)];
for i=2:Nside;
  xp(i)=-L/2;
  xm(i)=-L/2;
  yp(i)=-dy*i;
  ym(i)=-dy*(i-1);
  coord2=[xm(i),ym(i),xp(i),yp(i)];
coord=[coord;coord2];
end
for i=1+Nside:Nside+Nbott;
  i1=i-Nside;
  xp(i)=-L/2+dx*i1;
  xm(i)=-L/2+dx*(i1-1);
  yp(i)=-D;
  ym(i)=-D;
  coord2=[xm(i),ym(i),xp(i),yp(i)];
coord=[coord;coord2];
end
for i=1+Nside+Nbott:Nside+Nbott+Nside;
i1=i-Nside-Nbott;
  xp(i)=L/2;
  xm(i)=L/2;
  yp(i)=-D+dy*i1;
  ym(i)=-D+dy*(i1-1);
  coord2=[xm(i),ym(i),xp(i),yp(i)];
  coord=[coord;coord2];
end
save -ascii box.dat coord;
% plot geometry
xa=xm;
xa=[xm,xp(N)]
ya=ym;
ya=[ym,yp(N)]
hold on
axis ([-1.01 1.01 -1.1 0.01])
h1=plot(xa,ya,'k .')
plot(xa,ya,'k -')
axis off
get(h1);
set(h1,'MarkerSize',[25])
set(gca,'FontSize',20)
```

Figure 5 plots the discretisations of three different rectangular sections of width L and draught D where the latter defines the unit length in the calculations below.

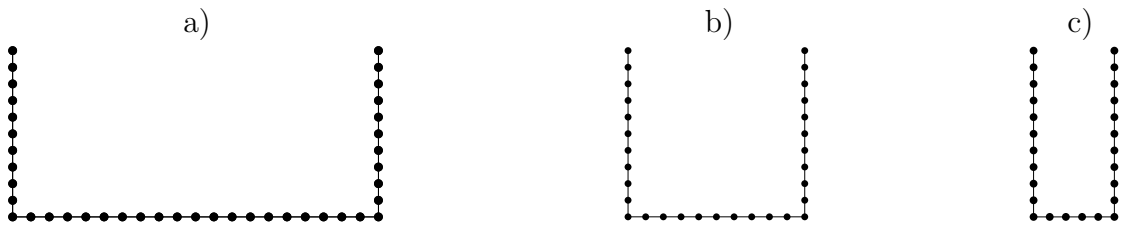

Figure 5: Discretisation of rectangular ship section of beam L and draught D with a) $D = 1$, $L = 2$, 10 segments on each vertical side, 20 segments on the bottom, and b) $D = 1$, $L = 1$, 10 segments on each vertical side, 10 segments on the bottom, and c) $D = 1$, $L = 0.5$, 10 segments on each vertical side, 5 segments on the bottom.

5.3 The wave Green function in two dimensions

The two-dimensional wave Green function where $g(x, y, t) = Re\Big(G(x, y)e^{\mathrm{i}\omega t}\Big)$ and $\nu = \omega^2/g$, reads

$$G = \log(r/r_1) \; + \; Re(f_1) \; + \; \mathrm{i}\, Re(f_2), \tag{67}$$

where $r = \sqrt{(x-\bar{x})^2 + (y-\bar{y})^2}$ and $r_1 = \sqrt{(x-\bar{x})^2 + (y+\bar{y})^2}$ the image with respect to $y = 0$, and

$$f_1 = 2\, PV \int_0^\infty \frac{e^{-\mathrm{i}k(z-\bar{\zeta}^*)}}{\nu - k} dk = -2e^Z(E_1(Z) + \log Z - \log(-Z)), \tag{68}$$

$$f_1 \to \pm 2\pi \mathrm{i} e^Z, \quad x - \bar{x} \to \pm\infty \tag{69}$$

$$f_2 = 2\pi e^Z, \tag{70}$$

$$Z = \nu(y + \bar{y}) - \mathrm{i}\nu(x - \bar{x}), \tag{71}$$

$$\frac{\partial G}{\partial x} = \frac{x-\bar{x}}{r^2} \; + \; \frac{x-\bar{x}}{r_1^2} \; + \; \nu\,[\, Im(f_1) \; + \; \mathrm{i}\, Im(f_2)\,], \tag{72}$$

$$\frac{\partial G}{\partial y} = \frac{y-\bar{y}}{r^2} \; + \; \frac{y+\bar{y}}{r_1^2} + \; \nu\,[\, Re(f_1) \; + \; \mathrm{i}\, Re(f_2)\,]. \tag{73}$$

The function E_1 in (68) is the exponential integral and is in matlab and python obtained by writing expint(Z).

In (68) $z = x + \mathrm{i}y$, $\bar{\zeta}^* = \bar{x} - \mathrm{i}\bar{y}$ and * denotes complex conjugate.

5.4 Test of the integral equation in the diffraction problem

The incoming wave potential reads $\phi_0 = (\mathrm{i}g/\omega)\varphi_0$ where $\varphi_0 = e^{\nu(y - \mathrm{i}x)}$. It is possible to show that the incoming wave potential satisfies

$$\pi\varphi_0 + \int_{S_B} \varphi_0 \frac{\partial G}{\partial n} dS = \int_{S_B} G \frac{\partial \varphi_0}{\partial n} dS, \tag{74}$$

for $(\bar{x}, \bar{y})$ on S_B where $\partial\varphi_0/\partial n = \nu(n_2 - \mathrm{i}n_1)\varphi_0$ and where S_B is the wetted surface of the body. The Green function is given in (67)– (73) above.

5.5 Discretisation of the integral equation

Equation (74) is discretised by subdividing the body boundary S_B into a number of N segments where $S_B = \sum_{m=1}^{N} S_m$, where each S_m is defined by the start coordinate, (x_m^-, y_m^-), and the end coordinate, (x_m^+, y_m^+). The centroid of the segment is defined by $(\bar{x}_m, \bar{y}_m) = (1/2)[(x_m^- + x_m^+, y_m^- + y_m^+)]$. Discretisation of the left hand side (L.H.S) of (74) gives

$$L.H.S = \pi\varphi_0(\bar{x}_n, \bar{y}_n) + \sum_{m=1}^{N} \varphi_0(\bar{x}_m, \bar{y}_m) \int_{S_m} \frac{\partial G}{\partial n} dS. \tag{75}$$

The contributions from the log-terms are obtained analytically obtaining a high accuracy, by

$$\begin{aligned} &\int_{S_m} \frac{\partial}{\partial n}\Big(\log r + \log r_1 \Big) dS \\ &= -Im\Big(\log[x + \mathrm{i}y - (\bar{x}_n + \mathrm{i}\bar{y}_n)]\Big|_{x_m^- + \mathrm{i}y_m^-}^{x_m^+ + \mathrm{i}y_m^+} \Big) - Im\Big(\log[x + \mathrm{i}y - (\bar{x}_n - \mathrm{i}\bar{y}_n)]|_{x_m^- + \mathrm{i}y_m^-}^{x_m^+ + \mathrm{i}y_m^+} \Big) \end{aligned} \tag{76}$$

where (x_m^-, y_m^-) and (x_m^+, y_m^+) denote the start and end point, respectively, of the segment S_m.

The integral over the wave part of $\partial G/\partial n$ is obtained by the midpoint rule giving

$$\simeq \Delta S_m \Big(n_1 \nu [\, Im(f_1) \, + \, \mathrm{i}\, Im(f_2) \,] + n_2 \nu \, [\, Re(f_1) \, + \, \mathrm{i}\, Re(f_2) \,] \Big) \Big|_{(\bar{x}_m, \bar{y}_m)} \tag{77}$$

Discretisation of the right hand side (R.H.S) of (74) gives

$$R.H.S = \sum_{m=1}^{N} \frac{\partial \varphi_0}{\partial n}\Big|_{(\bar{x}_m, \bar{y}_m)} \int_{S_m} G dS, \tag{78}$$

where $\int_{S_m} \log r dS$ is integrated by the two-points Gauss rule and the other terms by the mid point rule. The matlab script below illustrates the check (74) for the rectangular section in figure 5a and $\nu D = \omega^2 D/g = 1.7$. The numerical results in figure 6 compares the real and imaginary parts of the L.H.S in (75) and R.H.S in (78). The comparison is excellent along the box section indicating the robustness of the method of integral equations for the present purpose. Some minor inaccuracies observed at the sections close to the free surface are reduced by an increased resolution.

```
nu=1.7;
% characteristics of geometry
load -ascii box.dat
xm=box(:,1);
ym=box(:,2);
xp=box(:,3);
yp=box(:,4);
NN=40;
in=linspace(1,NN,NN);
```

```
dx=xp-xm;
dy=yp-ym;
ds=((dx).^2+(dy).^2).^(1/2);
bx=0.5*(xm+xp);
by=0.5*(ym+yp);
n1=-(yp-ym)./ds;
n2=(xp-xm)./ds;
% points for Gauss integration on each segment
xg1=-0.5*dx/sqrt(3)+bx;
xg2=0.5*dx/sqrt(3)+bx;
yg1=-0.5*dy/sqrt(3)+by;
yg2=0.5*dy/sqrt(3)+by;
% incoming wave potential
phi0=exp(nu*(by-complex(0,1)*bx));
phi0n=nu*(n2-complex(0,1)*n1).*phi0;
% contributions to integral equation, rhs stores rhs, lhs stores lhs
for i=1:NN
  for j=1:NN
% rhs, log(r) term with 2pts Gauss quadrature
    xa1=xg1(j)-bx(i);
    xa2=xg2(j)-bx(i);
    ya1=yg1(j)-by(i);
    ya2=yg2(j)-by(i);
    ra1=sqrt(xa1*xa1+ya1*ya1);
    ra2=sqrt(xa2*xa2+ya2*ya2);
    g0=(log(ra1)+log(ra2))*0.5;
% all other terms with midpoint rule
    xa=bx(j)-bx(i);
    yb=by(j)+by(i);
    rb=sqrt(xa*xa+yb*yb);
    g1=-log(rb);
    zz=nu*(yb-complex(0,1)*xa);
    f1=-2*exp(zz)*(expint(zz)+log(zz)-log(-zz));
    f2=2*pi*exp(zz);
    g2=real(f1)+complex(0,1)*real(f2);
    gg(i,j)=(g0+g1+g2)*ds(j);
% lhs
    arg0=imag(log((xm(j)-bx(i)+complex(0,1)*(ym(j)-by(i)))/
(xp(j)-bx(i)+complex(0,1)*(yp(j)-by(i)))));
    if j-i == 0
      arg0=pi;
    end
    arg1=imag(log((xm(j)-bx(i)+complex(0,1)*(ym(j)+by(i)))/
(xp(j)-bx(i)+complex(0,1)*(yp(j)+by(i)))));
    help1=(n1(j)* (imag(f1)+complex(0,1)*imag(f2)) +n2(j)*
(real(f1)+complex(0,1)*real(f2)) )*nu*ds(j);
```

```
    ss(i,j)=(arg0+arg1+help1);
  end
end
rhs=gg*phi0n;
lhs=ss*phi0;
hold on
plot(in,real(rhs),'k -')
g0=plot(in,real(lhs),'k .')
plot(in,imag(rhs),'k --')
g1=plot(in,imag(lhs),'k +')
get(g0)
get(g1)
set(g0,'MarkerSize',[12])
set(g1,'MarkerSize',[7])
set(gca,'FontSize',20)
```

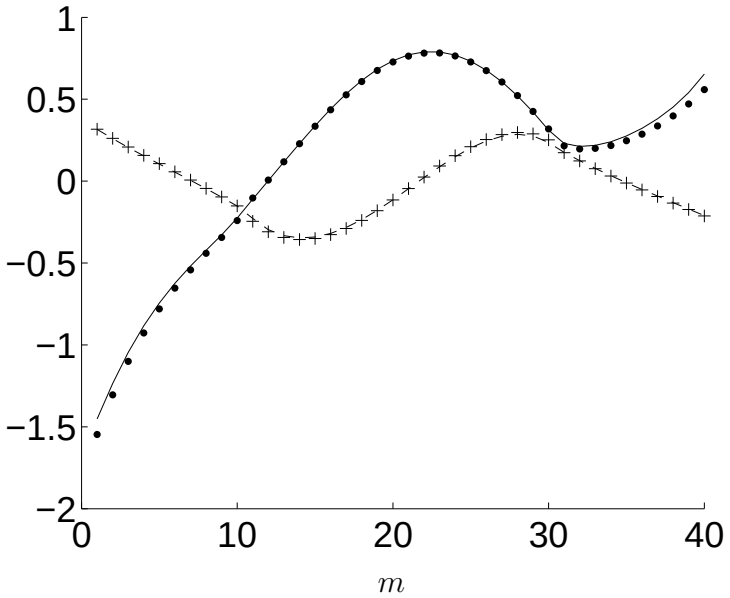

Figure 6: Real (——) and imaginary (− − −) parts of the R.H.S in (78), and real and imaginary parts (symbols) of the L.H.S in (75), as function of the section number S_m, $m = 1, .., N$ with $N = 40$, for the rectangular section in figure 5a with $\nu D = \omega^2 D/g = 1.7$ where D is the draught of the box and the width is $L = 2D$.

5.6 The radiation problem

In the radiation problem there are no incoming waves. The wave motion is driven by the oscillatory motion of the geometry. The radiation potential in two dimensions becomes

$$\Phi_R(x, y, t) = Re\Big(\sum_j \mathrm{i}\omega\xi_j \phi_j(x, y) e^{\mathrm{i}\omega t} \Big), \tag{79}$$

where the sum is over the modes: sway ($j = 1$), heave ($j = 2$) and roll ($j = 6$), where ξ_j denotes the complex motion amplitude in the respective modes. The potentials ϕ_j satisfy the Laplace equation as well as the same boundary conditions as the Green function, at the free surface and at infinity. The kinematic body boundary condition reads:

$$\frac{\partial \phi_j}{\partial n} = n_j \quad \text{at} \quad S_B, \tag{80}$$

where (n_1, n_2) denotes the unit normal at S_B pointing out of the fluid and $n_6 = xn_2 - yn_1$. The potentials ϕ_j are expressed in terms of integral equations giving for an evaluation point for $(\bar{x}, \bar{y})$ on the wetted body surface S_B

$$-\pi\phi_j + \int_{S_B} \phi_j \frac{\partial G}{\partial n} dS = \int_{S_B} G \frac{\partial \phi_j}{\partial n} dS, \tag{81}$$

where $\partial\phi_j/\partial n = n_j$. Note that equation (81), where $-\pi$ appears as a prefactor of the first term on the left hand side, differs from the test case in equation (74) where $+\pi$ appears as a prefactor of the first term on the left hand side. The reason for the $+\pi$ factor in (74) is discussed in a separate problem.

The outgoing waves are evaluated using the far field form of the Green function. For an evaluation point $(\bar{x}, \bar{y})$ in the fluid, not on the wetted body surface, we have

$$2\pi\phi_j(\bar{x}, \bar{y}) = \int_{S_B} \Big(\phi_j \frac{\partial G}{\partial n} - G \frac{\partial \phi_j}{\partial n}\Big) dS, \tag{82}$$

where in the far field $G = Re(f_1) + \mathrm{i}Re(f_2)$, $f_1 = \pm 2\pi \mathrm{i} e^Z$ (for $x - \bar{x} \to \pm\infty$), $f_2 = 2\pi e^Z$ and $Z = \nu(y + \bar{y}) - \mathrm{i}\nu(x - \bar{x})$. The behaviour of ϕ_j for $\bar{x} \to \pm\infty$ reads

$$\phi_j \to A_j^{\pm\infty} e^{\nu(\bar{y} \mp \mathrm{i}\bar{x})}, \quad \bar{x} \to \pm\infty, \tag{83}$$

where the complex constants $A_j^{\pm\infty}$ are obtained as integrals over the wetted body surface using (82) giving

$$A_j^{\pm\infty} = \mathrm{i} \int_{S_B} \Big[\phi_j \Big(n_1 \frac{\partial}{\partial x} + n_2 \frac{\partial}{\partial y}\Big) - n_j\Big] e^{\nu(y \pm \mathrm{i}x)}, \quad \bar{x} \to \pm\infty. \tag{84}$$

The corresponding wave elevation is obtained from the radiation potential by

$$\eta(\bar{x}, t) = -\frac{1}{g} \frac{\partial \Phi_R}{\partial t} = \sum_j Re\Big(amp_j^{\pm\infty} e^{\mp \mathrm{i}\nu\bar{x} + \mathrm{i}\omega t}\Big), \tag{85}$$

where the complex wave amplitudes $amp_j^{\pm\infty}$ are related to the complex constants $A_j^{\pm\infty}$ in (84) by

$$amp_j^{\pm\infty} = \frac{\omega^2}{g} \xi_j A_j^{\pm\infty} \quad \text{(not sum over } j\text{)}. \tag{86}$$

Once the solution of the integral equation (81) is obtained, the far field wave amplitudes $amp_j^{\pm\infty}$ and $A_j^{\pm\infty}$ in (86) as well as the force and moment on the body may be

evaluated. The latter are expressed in terms of the added mass and damping coefficients by

$$F_i(t) = \sum_j \Big(- \dot{U}_j a_{ji} - U_i b_{ji} \Big) = \int_{S_B} \Big(- \rho \frac{\partial \Phi_R}{\partial t} \Big) n_i dS = \sum_j Re \Big(- (\mathrm{i}\omega)^2 \xi_j f_{ji} e^{\mathrm{i}\omega t} \Big), \quad (87)$$

$(j = 1, 2, 6)$ where

$$f_{ji} = \rho \int_{S_B} \phi_j n_i dS = a_{ji} + \frac{b_{ji}}{\mathrm{i}\omega}. \quad (88)$$

5.6.1 Obtaining the damping force from the far field energy flux

The time-averaged work done by the force on the body, given by

$$\overline{W} = -\overline{F_j U_j} = \frac{1}{2} \omega^2 |\xi_j|^2 b_{jj}, \quad (89)$$

results in the outgoing waves at $\bar{x} = \pm\infty$ and a corresponding mean energy flux ($En.Flux$) given by

$$En.Flux = \overline{E^{\infty}} c_g + \overline{E^{-\infty}} c_g = \Big(\frac{1}{2} \rho g |amp^{\infty}|^2 + \frac{1}{2} \rho g |amp^{-\infty}|^2 \Big) \frac{g}{2\omega}, \quad (90)$$

where $\overline{W}$ balances the $En.Flux$ and where a bar denotes time-average. This gives

$$\frac{b_{jj}}{\rho\omega} = \frac{g^2}{2\omega^4} \left(\left| \frac{amp_j^{\infty}}{\xi_j} \right|^2 + \left| \frac{amp_j^{-\infty}}{\xi_j} \right|^2 \right) = \frac{1}{2} (|A_j^{\infty}|^2 + |A_j^{-\infty}|^2), \quad (91)$$

where (86) has been used. If the geometry is symmetrical with respect to $x = 0$ it can be shown that $|A_j^{\infty}| = |A_j^{-\infty}|$.

5.6.2 Numerical solution of the integral equation

The discretisation procedures and matlab-script outlined in Section 5.5, solving (74) numerically, may be modified to obtain the solution of (81). The first modification is to put $-\pi\phi_j$ instead of $\pi\phi_0$ in the first term on the L.H.S. Next the boundary condition of the radiation problem has to be applied. For, e.g., the heave problem the parts of the script conerning the left hand side of the equation as well as its solution are modified to:

```
% lhs
    arg0=imag(log((xm(j)-bx(i)+complex(0,1)*(ym(j)-by(i)))/
(xp(j)-bx(i)+complex(0,1)*(yp(j)-by(i)))));
    if j-i == 0
      arg0=-pi;
    end
    arg1=imag(log((xm(j)-bx(i)+complex(0,1)*(ym(j)+by(i)))/
(xp(j)-bx(i)+complex(0,1)*(yp(j)+by(i)))));
    help1=(n1(j)* (imag(f1)+complex(0,1)*imag(f2)) +n2(j)*
```

```
(real(f1)+complex(0,1)*real(f2)) )*nu*ds(j);
    ss(i,j)=(arg0+arg1+help1);
  end
end
rhs=gg*n2;
phi2=ss\rhs;
```

where the array phi2 contains the numerical representation of ϕ_2 at the midpoint of each segment S_m of S_B. The added mass and damping coefficients are evaluated by

```
ff22=phi2.*n2.*ds;
sff22=sum(ff22);
```

where $a_{22}/(\rho D^2) = Re(\text{sff22})$ and $b_{22}/(\rho\omega D^2) = -Im(\text{sff22})$. The complex far field amplitudes of the potential are evaluated by

```
phi0=exp(nu*(by-complex(0,1)*bx));
AM2=complex(0,1)*(phi2.*(nu*n2-nu*complex(0,1)*n1)-n2).*phi0.*ds;
AP2=complex(0,1)*(phi2.*(nu*n2+nu*complex(0,1)*n1)-n2).*conj(phi0).*ds;
sAM2=sum(AM2);
sAP2=sum(AP2);
```

where sAM2=$A_2^{-\infty}$ and sAP2=A_2^{∞}. Figure 7 plots the added mass and damping coefficients in the heave mode of motion of a rectangular section of width twice the draught. The damping coefficient is obtained by the local pressure integration as well as by the energy flux in the far field, with excellent comparison. It may be shown that $b_{22}/(\rho\omega D^2) \to 4$ as $\omega^2 D/g \to 0$ in this case. The added mass coefficient in heave tends to infinity in the long wavelength limit. The numerical solution is illposed at $\omega^2 D/g \approx 1.73$ corresponding the the first irregular frequency of the integral equation. This corresponds to the first mode of the internal homogeneous Dirichelt problem of the section and is not discussed in this course.

5.7 The diffraction problem

In the diffraction problem the geometry is held fixed. The incoming wave field interacts with the geometry resulting in a field of scattered waves. These are superposed on the incoming wave field. In two dimensions the diffraction potential is represented by

$$\Phi_D(x,y,t) = Re\Big(A(\phi_0(x,y) + \phi_7(x,y))e^{\mathrm{i}\omega t}\Big), \tag{92}$$

where A denotes the amplitude of the incoming waves, ϕ_0 the incoming wave potential and ϕ_7 the scattering potential. The sum $\phi_D = \phi_0 + \phi_7$ is also commonly used. An incoming wave field propagating along the positive x-axis is represented by, in the case of deep water,

$$\phi_0(x,y) = \frac{\mathrm{i}g}{\omega} e^{\nu y - \mathrm{i}\nu x}, \tag{93}$$

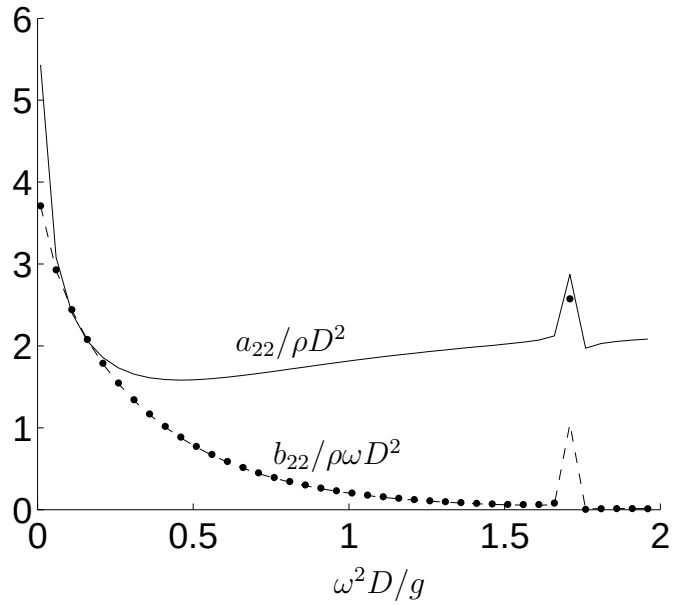

Figure 7: Added mass a_{22} (——) and damping b_{22} (− − −) of the rectangular section in figure 5a. b_{22} obtained by (91) (dots).

where $\nu = \omega^2/g$. The scattering potential ϕ_7 is Laplacian and satisfies the same conditions as the Green function at the free surface and at the control surfaces at $x = \pm\infty$. The kinematic condition at the nonmoving body boundary reads

$$\frac{\partial \phi_D}{\partial n} = \frac{\partial \phi_0}{\partial n} + \frac{\partial \phi_7}{\partial n} = 0 \quad \text{at } S_B, \tag{94}$$

giving that $\partial\phi_7/\partial n = -\partial\phi_0/\partial n$.

5.7.1 Integral equation in the diffraction problem

The potential ϕ_7 is unknown, while ϕ_0 is given. The best way to find ϕ_7 is to solve an integral equation for the sum $\phi_D = \phi_0 + \phi_7$. It may be shown that this is obtained by

$$-\pi\phi_D(\bar{x},\bar{y}) + \int_{S_B} \phi_D \frac{\partial G}{\partial n} dS = -2\pi\phi_0, \tag{95}$$

for $(\bar{x},\bar{y})$ on S_B. A numerical solution of this equation is obtained by the script

```
load -ascii box.dat
xm=box(:,1);
ym=box(:,2);
xp=box(:,3);
yp=box(:,4);
nu=1.5;
NN=40;
% characteristics of geometry
dx=xp-xm;
```

```
dy=yp-ym;
ds=((dx).^2+(dy).^2).^(1/2);
bx=0.5*(xm+xp);
by=0.5*(ym+yp);
n1=-(yp-ym)./ds;
n2=(xp-xm)./ds;
% incoming wave potential
phi0=exp(nu*(by-complex(0,1)*bx));
% contributions to integral equation, rhs stores rhs, lhs stores lhs
for i=1:NN
  for j=1:NN
    xa=bx(j)-bx(i);
    yb=by(j)+by(i);
    zz=nu*(yb-complex(0,1)*xa);
    f1=-2*exp(zz)*(expint(zz)+log(zz)-log(-zz));
    f2=2*pi*exp(zz);
    g2=real(f1)+complex(0,1)*real(f2);
% lhs
    arg0=imag(log((xm(j)-bx(i)+complex(0,1)*(ym(j)-by(i)))/(xp(j)-bx(i)
+complex(0,1)*(yp(j)-by(i)))));
    if j-i == 0
      arg0=-pi;
    end
    arg1=imag(log((xm(j)-bx(i)+complex(0,1)*(ym(j)+by(i)))/(xp(j)-bx(i)
+complex(0,1)*(yp(j)+by(i)))));
    help1=(n1(j)* (imag(f1)+complex(0,1)*imag(f2)) +n2(j)*
(real(f1)+complex(0,1)*real(f2)) )*nu*ds(j);
    ss(i,j)=(arg0+arg1+help1);
  end
end
rhsD=-2*pi*phi0;
phiD=ss\rhsD;
```

where the array phiD stores the potential ϕ_D along S_B.

5.7.2 The exciting force

The wave force on the geometry in the diffraction problem is obtained by

$$F_j(t) = \int_{S_B} Re\Big(-\rho \frac{\partial \Phi_D}{\partial t}\Big) n_j dS = Re\Big(A X_j e^{\mathrm{i}\omega t}\Big), \tag{96}$$

where

$$X_j = -\mathrm{i}\omega\rho \int_{S_B} (\phi_0 + \phi_7) n_j dS, \tag{97}$$

denotes the exciting force where $j = 1, 2, 6$ in the two-dimensional case. The force in the vertical direction is evaluated by the script

```
XX2=phiD.*n2.*ds;
sXX2=sum(XX2);
```

where the complex variable sXX2 multiplied by $-\mathrm{i}\omega\rho$ gives the exciting force X_2.

5.7.3 Haskind relations

The exciting force is obtained in several variants. These provide useful checks of the evaluations. By using the body boundary condition for the radiation potentials, i.e., $n_j = \partial\phi_j/\partial n$, we obtain

$$X_j = -\mathrm{i}\omega\rho \int_{S_B} (\phi_0 + \phi_7)\frac{\partial\phi_j}{\partial n} dS = -\mathrm{i}\omega\rho \int_{S_B} \Big(\phi_0 \frac{\partial\phi_j}{\partial n} - \phi_j \frac{\partial\phi_0}{\partial n}\Big) dS, \tag{98}$$

where

$$\int_{S_B} \Big(\phi_7 \frac{\partial\phi_j}{\partial n} - \phi_j \frac{\partial\phi_7}{\partial n}\Big) dS = 0, \tag{99}$$

and the body boundary condition (94) have been used. By use of Greens theorem another time (98) may be expressed by integrals of the control surfaces at $x = \pm\infty$ giving

$$X_j = \mathrm{i}\omega\rho \int_{S_\infty} \Big(\phi_0 \frac{\partial\phi_j}{\partial n} - \phi_j \frac{\partial\phi_0}{\partial n}\Big) dS = \mathrm{i}\rho g A_j^{-\infty} \tag{100}$$

where $A_j^{-\infty}$ denotes the far field amplitude at $x = -\infty$ of the radiation potential ϕ_j where $\phi_j^{-\infty} = A_j^{-\infty} e^{\nu y + \mathrm{i}\nu x}$ at $x = -\infty$ while ϕ_0 is given in (93).

The exciting force X_2 in heave on the rectangular section of draught D and width $L = 2D$, obtained by the direct integration (97) as well as the Haskind relation (100) is shown in figure 8 where both methods give the same result and where the effect of the irregular frequency at $\omega^2 D/g \approx 1.73$ again is present.

Note from (100) that $|X_j|^2/(\rho g)^2 = |A_j^{-\infty}|^2$ while from the energy relation (90), for a geometry symmetrical about $x = 0$, we have $b_{jj}/\rho\omega = |A_j^{-\infty}|^2$ giving

$$\frac{b_{jj}}{\rho\omega} = \frac{|X_j|^2}{(\rho g)^2}. \tag{101}$$

The damping coefficient $b_{22}/\rho\omega$ in figure 7 is thus the square of the exciting force $|X_2|/\rho g$ in figure 8.

5.7.4 Approximations of the exciting force

Several approximations of the exciting force may be useful. The Froude Krylov force is defined by

$$X_j^{FK} = -\mathrm{i}\omega\rho \int_{S_B} \phi_0 n_j dS, \tag{102}$$

where in this approximation the effect of the scattering potential ϕ_7 is assmumed to be small and is omitted, which in some cases may be relevant.

For long waves with $\nu L << 1$ where L is the characteristic length of the geometry it may be shown that

$$X_2^{long\,wave} = \rho g S - \omega^2(a_{22} + \rho V) + \mathrm{i}\omega b_{22} \tag{103}$$

$$X_1^{long\,wave} = -\omega^2(a_{11} + \rho V) + \mathrm{i}\omega b_{11} \tag{104}$$

where V denotes the displaced mass of the geometry.

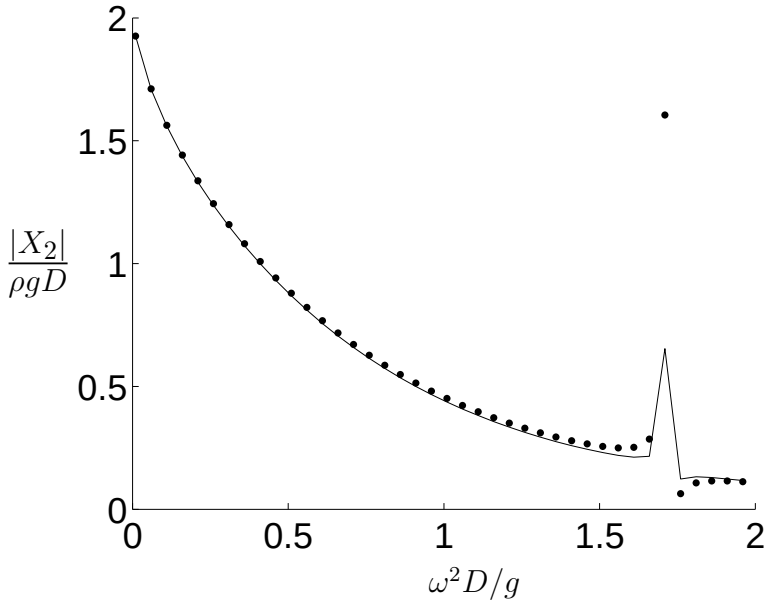

Figure 8: Exciting force $|X_2|$ in heave on a rectangular section by direct integration (——) and by the Haskind relation (dots). Draught D, width $L = 2D$.

5.8 Response in heave. Resonance

Consider the equation of motion in the case of the heave mode of motion only, given by

$$\Big(-\omega^2(m + a_{22}) + \mathrm{i}\omega b_{22} + c_{22}\Big)\xi_2 = AX_2, \tag{105}$$

where inversion gives

$$\frac{\xi_2}{A} = \frac{X_2}{c_{22} - \omega^2(m + a_{22}) + \mathrm{i}\omega b_{22}}, \tag{106}$$

where $c_{22} = \rho g S$ (S the water plane area of the geometry which in the two-dimensional case corresponds to the width of the geometry at the free surface) and where m denotes the mass of the geometry. In the case of a freely floating body the mass equals the buoyancy force. The functions X_2, a_{22}, b_{22} are evaluated above. The resonance frequency ω_n occurs where the hydrostatic restoring force balances the inertia forces, i.e., $c_{22} - \omega_n^2(m + a_{22}) = 0$. The resonance frequency for the freely floating two-dimensional rectangular section of width L and draugth D becomes

$$\omega_n^2 = \frac{g}{D}\ \frac{1}{1 + a_{22}/(\rho D L)}. \tag{107}$$

From the added mass calculations in figure 7 we obtain that $a_{22}/\rho D^2 \simeq 1.8$ for $\omega^2 D/g$ between 0.5 and 1 (and $L = 2D$) giving that $\omega_n^2 D/g \simeq 0.53$. The plot in figur 9 shows the heave response ξ_2/A as function of the wavenumber where the resonance is highlighted. It also shows an approximate calculation based on the analysis of a narrow rectangular box ($L << D$) detailed in Section 5.8.1 below. In figure 9b the approximate solution to the heave response with the added mass term included shows rather close corresponence to the full solution. This illustrates that correcting for the added mass effect is important both to calculate the correct resonance frequency as well as to calculate the heave response accurately at the other frequencies.

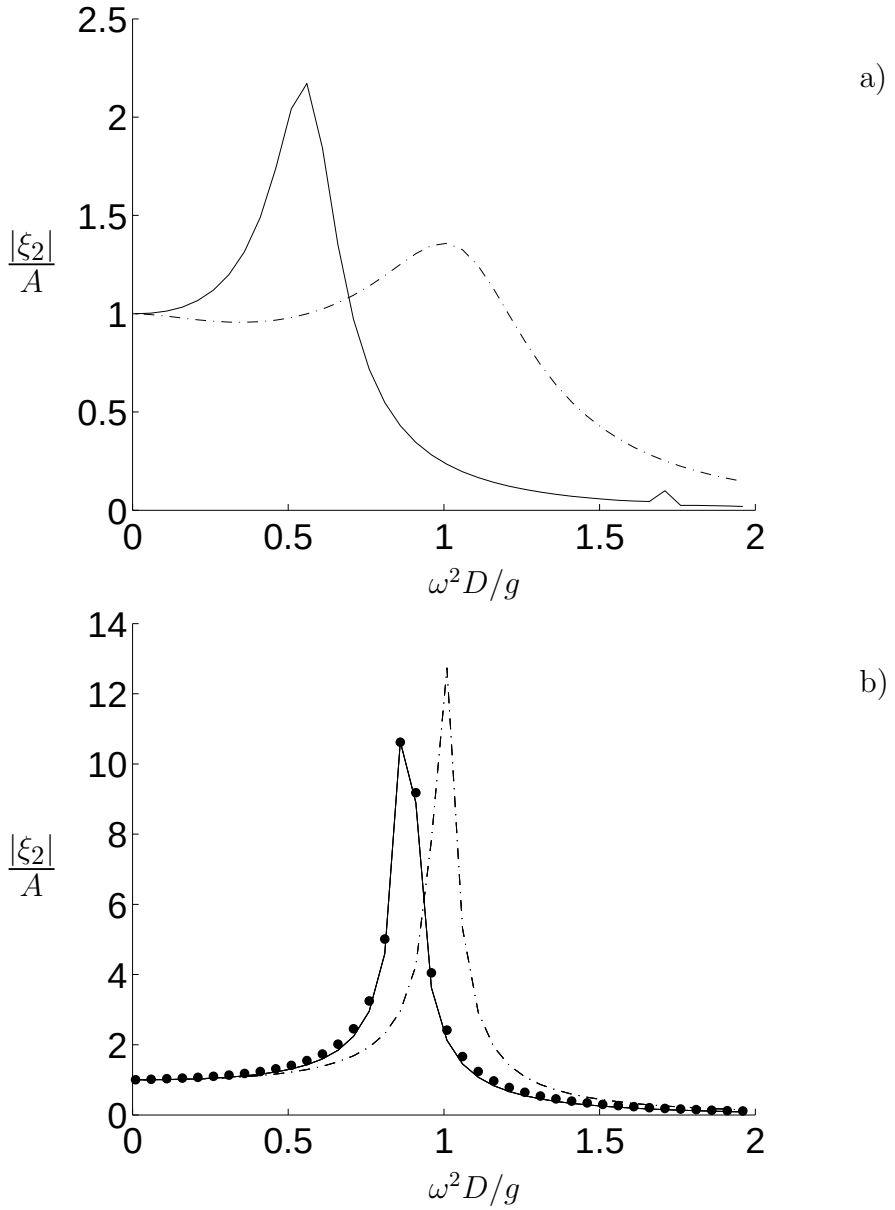

Figure 9: Response amplitude operator $|\xi_2/A|$ in heave on a rectangular section of draught D. Calculation of all terms (solid line). Approximation (dash-dots). Approximation with correction for added mass (large dots). a) Width $L = 2D$, b) width $L = 0.2D$.

5.8.1 Approximate analysis of a narrow box section

Consider the vertical exciting force, damping and vertical response of a two-dimensional box section of draught D and width L with $L/D << 1$. The exciting force is estimated by the Froude Krylov force

$$X_2^{FK} \simeq -\mathrm{i}\omega\rho \int_{S_B} \phi_0 n_2 dS \simeq \rho g L e^{-\nu D}, \tag{108}$$

where $\nu = \omega^2$. The damping coefficient is estimated from the Haskind relation giving

$$\frac{b_{22}}{\rho\omega} = L^2 e^{-2\nu D}. \tag{109}$$

The heave response is then estimated by

$$\frac{\xi_2}{A} \simeq \frac{\rho g L e^{-\nu D}}{\rho g L - \omega^2 m + \mathrm{i}\omega^2 \rho L^2 e^{-2\nu D}} = \frac{e^{-\nu D}}{1 - (\omega^2 D/g) + \mathrm{i}(\omega^2 L/g) e^{-2\nu D}}, \tag{110}$$

where $\omega_n^2 D/g = 1$ since the effect of added mass is not included in the evaluation.

5.9 Calculation of the response in a realistic sea state

The spectral components of an irregular sea are given by a wave spectrum, $S(\omega)$ where ω is the frequency. The JONSWAP spectrum is a recommended spectrum, given mathematically by

$$S(\omega) = 155 \frac{H_{1/3}^2}{T_1^4 \omega^5} e^{-944/(T_1^4\omega^4)} \, (3.3)^Y \quad [\mathrm{m^2 s}], \tag{111}$$

where $H_{1/3}$ is the significant wave height and T_1 is a mean wave period defined mathematically from the spectrum by $T_1 = 2\pi m_0/m_1$, where the moments are given by

$$m_k = \int_0^\infty \omega^k S(\omega) d\omega. \tag{112}$$

The significant wave height is often defined by

$$H_{1/3} = 4\sqrt{m_0}. \tag{113}$$

The remaining variables in (111) are defined by

$$Y^{-\left(\frac{0.191\omega T_1 - 1}{\sqrt{2}\sigma}\right)^2} \tag{114}$$

$$\sigma = 0.07 \quad (\omega T_1 \leq 5.24), \quad \sigma = 0.09 \quad (\omega T_1 \leq 5.24). \tag{115}$$

Note that another definition of a mean wave period is $T_2 = 2\pi\sqrt{m_0/m_2}$ where for the JONSWAP spectrum $T_1 = 1.086 T_2$.

The matlab-script below calculates the heave response amplitude operator of the rectangular section of with $L = 2D$.

The script also calculates the Jonswap spectrum where the mean wave period is put to 6 seconds, and the sample draught of the section is put to 15 meter.

Both functions are obtained in figure 10.

```
load -ascii outdat40.dat
nu=outdat40(:,1);
X2r40=outdat40(:,2);
X2i40=outdat40(:,3);
a2240=outdat40(:,8);
b2240=-outdat40(:,9);
dd40=2;
m2240=dd40;
rao40=(X2r40+complex(0,1)*X2i40)./(dd40-nu*m2240-nu.*a2240+complex(0,1)*nu.*b2240);
% choose D=15 m (and L=30 m), calculate frequency in seconds
om=sqrt(nu)'*sqrt(15/9.81);
% choose mean wave period T2=6 sec of the Jonswap spectrum
% mean wave period T1=1.086 T2
T2=6;
omt2=om*T2;
omt1=omt2*1.086;
% Calculate the Jonswap spectrum
NN=40;
for nn=1:NN;
sigma(nn)=0.07;
if omt1(nn) > 5.24;
sigma(nn)=0.09;
continue
end
end
YY=exp(-((0.191*omt1-1)./(sqrt(2)*sigma)).^2);
SS=(155./(omt1.^4.*omt2)).*exp(-944./(omt1.^4)).*(3.3).^YY;
hold on
axis([0 2 0 2.5])
g040=plot(nu,abs(rao40),'k -')
get(g040)
g5=plot(nu,T2*10*SS,'k -.');
get(g5);
set(g5,'MarkerSize',[10])
set(gca,'FontSize',20)
```

The standard deviation of the response, in an irregular sea given by a spectrum, $S(\omega)$, may be expressed by

$$\sigma_r^2 = \int_0^\infty S(\omega)|\xi_2/A|^2 d\omega, \tag{116}$$

where a calculation (script below) using the functions in figure 10, with $T = 6$ seconds and $D = 15$ m (and $L/D = 2$) gives $\sigma_r \simeq 0.358 H_{1/3}$. This means that if $H_{1/3} = 8$ m the standard deviation of the heave response is $\sigma_r \simeq 2.86$ m.

```
intresp=0.0;
```

```
for nn=1:NN-1;
aa=0.5*(SS(nn)+SS(nn+1));
bb=0.5*(abs(rao40(nn))^2+abs(rao40(nn+1))^2);
dom=om(nn+1)-om(nn);
intresp=intresp+aa*bb*dom*T2;
end
sqrt(intresp)
```

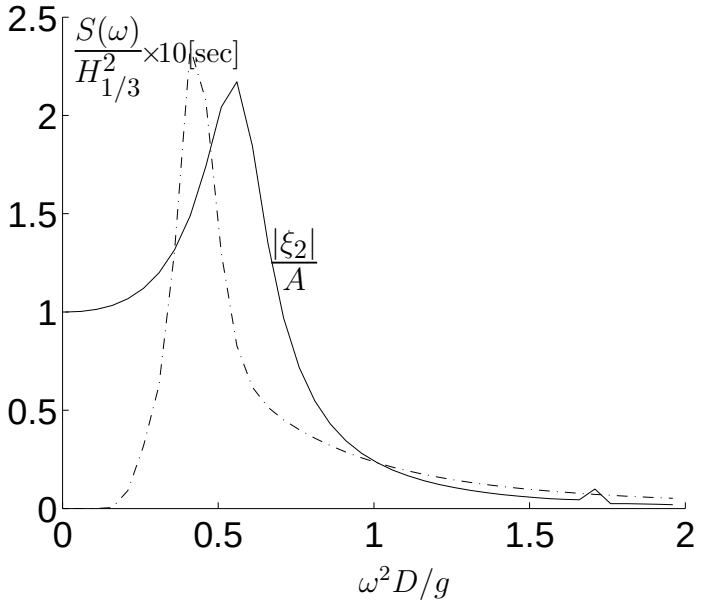

Figure 10: Response amplitude operator $|\xi_2/A|$ in heave on a rectangular section of draught $D = 15$ m and width $L = 30$ m (solid line). Jonswap spectrum $S(\omega)$ with $T_2 = 6$ seconds (dash-dots).

6 Student task. The forces and response of a heaving section in 2D

6.1 The BVP of the heave problem

• Formulate the boundary value problem (BVP) for the heaving potential ϕ_2 due to a geometry-section floating in the free surface, in two dimensions, where the radiation potential is given by

$$\Phi_R(x,y,t) = Re\Big(\mathrm{i}\omega\xi_2\phi_2(x,y)e^{\mathrm{i}\omega t}\Big). \tag{117}$$

where $\omega^2/g = K$, ξ_2 the (given) complex heave amplitude and ϕ_2 the complex potential in the heave mode of motion.

6.2 The BVP for the Green function

• Formulate the boundary value problem for the Green function G, where

$$g(x,y;\bar{x},\bar{y},t) = Re\Big(G(x,y;\bar{x},\bar{y})e^{\mathrm{i}\omega t}\Big), \tag{118}$$

$$G(x,y;\bar{x},\bar{y}) = \log r + H(x,y;\bar{x},\bar{y}), \tag{119}$$

and $r = \sqrt{(x-\bar{x})^2 + (y-\bar{y})^2}$.

In the formulation of this BVP, formulate the field equation, the bounday conditions at the free surface, at $x = \pm\infty$, and at $y \to -\infty$.

6.3 Integral equation

• Use Green's theorem to derive an integral equation for the heave problem with a free surface.

6.4 Integral equation (2)

The integral equation in section 6.3 becomes

$$-\pi\phi_2(\bar{x},\bar{y}) + \int_{S_B} \phi_2 \frac{\partial G}{\partial n} dS = \int_{S_B} G n_2 dS, \tag{120}$$

for $(\bar{x},\bar{y})$ on the body boundary S_B.

In the case when $(\bar{x},\bar{y})$ is in the fluid (not on S_B) the equation becomes (it is then not an integral equation)

$$2\pi\phi_2(\bar{x},\bar{y}) = \int_{S_B} \Big(\phi_2 \frac{\partial G}{\partial n} - G n_2\Big) dS, \tag{121}$$

6.5 Numerical solution of the integral equation

6.5.1 Discretisation of the wetted surface S_B

• Make a discretisation of the wetted part of a rectangular geometry of witdh L and draught D where D is chosen as unit length in the problem. Use N_2 as resolution along the vertical sides and N_1 as resolution along the bottom of the rectangle, where $\Delta y = D/N_2$ and $\Delta x = L/N_1$.

• Make discretisations for three different geometries with $L/D = 2, 1$ and 0.1. It sufficies to use $N_2 = 10$. Use a similar resolution along the bottom and $N_1 = 5$ for the thin rectangle.

The equation to be solved is

$$-\pi\phi_2 + \int_{S_B} \phi_2 \frac{\partial G}{\partial n} dS = \int_{S_B} G n_2 dS, \tag{122}$$

6.5.2 Solution of a relation where all terms are known

A variant of the equation (122) is (shall not be derived)

$$\pi\varphi_0 + \int_{S_B} \varphi_0 \frac{\partial G}{\partial n} dS = \int_{S_B} G \frac{\partial \varphi_0}{\partial n} dS, \tag{123}$$

where $\varphi_0 = e^{Ky - \mathrm{i}Kx}$ and $K = \omega^2/g$, where all contributions in the terms in (123) are known.

• Formulate a discrete version of (123) using the procedures described in the Lecture Notes.

• Make a numerical implementation of (123) using analytical integration of the normal derivatives of the log-terms (see the Lecture Notes), two-point Gauss integration of the $\log r$ contribution and mid-point rule for the remaining terms.

• Test the numerical implementation for one of the rectangular geometries for a given $KD = 1.2$ or 0.9. Illstrate by plots that

$$Re(L.H.S) = Re(R.H.S),$$
$$Im(L.H.S) = Im(R.H.S),$$

along the wetted body surface S_B.

6.5.3 Solution of the heave problem

• Then solve (122) numerically for the three different rectangular geometries.

6.6 Far field behavior of ϕ_2

The potential ϕ_2 has far field form

$$\phi_2(\bar{x}, \bar{y}) \to A_2^{-\infty} e^{K\bar{y} + \mathrm{i}K\bar{x}}, \quad \bar{x} \to -\infty, \tag{124}$$
$$\phi_2(\bar{x}, \bar{y}) \to A_2^{\infty} e^{K\bar{y} - \mathrm{i}K\bar{x}}, \quad \bar{x} \to \infty, \tag{125}$$

where $K = \omega^2/g$.

• Use (121) to derive expressions for $A_2^{-\infty}$ and A_2^{∞}.

6.7 The outgoing wave amplitudes

The wave elevation of the outgoing waves has (complex) amplitudes

$$amp_2^{-\infty} = \xi_2 A_2^{-\infty}\omega^2/g, \tag{126}$$

$$amp_2^{\infty} = \xi_2 A_2^{\infty}\omega^2/g. \tag{127}$$

The mean energy flux of the outgoing waves is given by

$$En.Flux = \bar{E}^{\infty}c_g + \bar{E}^{-\infty}c_g, \tag{128}$$

where $\bar{E}^{\pm\infty} = (1/2)\rho g|amp_2^{\pm\infty}|^2$ is the mean energy density of the outgoing waves and $c_g = \partial\omega/\partial K$ the group velocity. (To show this is not needed.)

6.8 Added mass and damping

• Use the numerical solution of ϕ_2 along the wetted body surface S_B to calculate the added mass a_{22} and damping b_{22} for the wavenumber range $0 < KD = \omega^2 D/g < 2$ for the three geometries.

• Calculate also b_{22} from the energy balance

$$\frac{1}{2}|\xi_2|^2\omega^2 b_{22} = \bar{E}^{-\infty}c_g + \bar{E}^{\infty}c_g. \tag{129}$$

6.9 Approximate solution

• Solve problem 6.17 in Newman for the 2D case obtaining approximations of the exciting force and damping force. Compare the approximate solution to the full calculation of b_{22}.

Hint: In the calculation of the exciting force in problem 6.17 use of the Froude-Krylov approximation is made, obtaining, in the 2D case,

$$X_2^{FK} = -\mathrm{i}\omega\rho\int_{S_B}\phi_0 n_2 dS = \rho g\int_{-L/2}^{L/2} e^{-KD-\mathrm{i}Kx}dx = \rho g L e^{-KD}\,\frac{\sin(KL/2)}{KL/2} \tag{130}$$

6.10 The diffraction problem

In the diffraction problem the geometry is fixed. The fluid motion is given by the velocity potential

$$\Phi_D(x,y,t) = Re\Big(A\phi_D(x,y)e^{\mathrm{i}\omega t}\Big), \tag{131}$$

where A is the amplitude of the incoming waves, $\phi_D(x,y) = \phi_0(x,y) + \phi_7(x,y)$, $\phi_0 = (\mathrm{i}g/\omega)e^{Ky-\mathrm{i}Kx}$ denotes the potential of the incoming waves (given) and ϕ_7 is the scattering

potential (unknown). Further, $K = \omega^2/g$. The integral equation to determine the sum $\phi_D = \phi_0 + \phi_7$ for a point $(\bar{x}, \bar{y})$ on S_B is

$$-\pi\phi_D(\bar{x},\bar{y}) + \int_{S_B} \phi_D \frac{\partial G}{\partial n} dS = -2\pi\phi_0(\bar{x},\bar{y}). \tag{132}$$

• Solve (132) numerically for the three rectangular sections.

6.10.1 The exciting force

• Obtain numerically the exciting force

$$\frac{X_2}{\rho g} = -\frac{\mathrm{i}\omega}{g} \int_{S_B} \phi_D n_2 dS. \tag{133}$$

6.10.2 Haskind relations

The exciting force may be obtained by the Haskind relations which are obtained in various variants. These provide checks on the computations. The Haskind relations are derived by the following:

$$\frac{X_2}{\mathrm{i}\omega\rho} = -\int_{S_B} (\phi_0 n_2 + \phi_7 n_2) dS = -\int_{S_B} \Big(\phi_0 \frac{\partial \phi_2}{\partial n} + \phi_7 \frac{\partial \phi_2}{\partial n}\Big) dS, \tag{134}$$

where the boundary condition $\partial\phi_2/\partial n = n_2$ is used. Further, the potentials ϕ_2 and ϕ_7 satisfy the same boundary conditions at: a) the free surface where $-\omega^2\phi_{2,7} + g\partial\phi_{2,7}/\partial y = 0$the at $y = 0$, b) in the far field at $x = \pm\infty$, $\partial\phi_{2,7}/\partial n = -\mathrm{i}K\phi_{2,7}$, $x \pm \infty$, and c) for $y \to -\infty$ where $|\nabla\phi_{2,7} \to 0|$. This gives that

$$\int_{S_B} \Big(\phi_7 \frac{\partial \phi_2}{\partial n} - \phi_2 \frac{\partial \phi_7}{\partial n}\Big) dS = 0. \tag{135}$$

Combining with (134), using that $\partial\phi_7/\partial n = -\partial\phi_0/\partial n$ (from the body boundary condition in the diffraction problem), gives

$$\frac{X_2^{Haskind,1}}{\mathrm{i}\omega\rho} = -\int_{S_B} \Big(\phi_0 \frac{\partial \phi_2}{\partial n} - \phi_2 \frac{\partial \phi_0}{\partial n}\Big) dS, \tag{136}$$

or, alternatively, by the far field integrals, using Green's theorem,

$$\frac{X_2^{Haskind,2}}{\mathrm{i}\omega\rho} = \int_{S_\infty} \Big(\phi_0 \frac{\partial \phi_2}{\partial n} - \phi_2 \frac{\partial \phi_0}{\partial n}\Big) dS. \tag{137}$$

In the latter the integration is performed at $x = -\infty$ and $x = \infty$. In two dimensions the two integrals (136) and (137) are exactly the same.

The far field of ϕ_2 is given by

$$\phi_2 = A_2^{\pm} e^{Ky \mp \mathrm{i}Kx}, \quad x \to \pm\infty, \tag{138}$$

where

$$A_2^{\pm\infty} = \mathrm{i}\int_{S_B}\Big[\phi_2\Big(n_1\frac{\partial}{\partial x} + n_2\frac{\partial}{\partial y}\Big) - n_2\Big]e^{Ky\mp \mathrm{i}Kx}dS. \tag{139}$$

• Show that

$$\frac{X_2^{Haskind,2}}{\rho g} = \mathrm{i}A_2^{-\infty}. \tag{140}$$

• Calculate the exciting force $X_2/\rho g$ for the three sections using the direct pressure integration (133), the version 1 of the Haskind relation (136) and the version 2 of the Haskind relation (140).

• Compare also to the Froude Krylov approximation in (130). Perform calculations for the wavenumber range $0 < KD < 2$.

6.11 Body response in heave

• Formulate the equation of motion in the heave mode of motion (assuming no motion in the other modes). Obtain an expression for the response $|\xi_2|/A$.

6.11.1 Resonance frequency

• Determine the resonance frequency of the three rectangular sections with $L/D = 2, 1$ and 0.1.

6.11.2 Response as function of the frequency

• Plot $|\xi_2/A|$ as function of the wavenumber for each of the three geometries for $0 < KD < 2$.

6.11.3 Response as function of the frequency (2)

• Include also in the plots the response calculated by the Froude Krylov approximation X_2^{FK}, with b_{22} obtained by the Haskind relation based on X_2^{FK} and where the effect of the added mass a_{22} is neglected.

6.11.4 Response as function of the frequency (3)

• Use the approximate method with a_{22} included in the calculation.

6.12 Write a conclusion

• Write down, point wise, in 5 main points, the main conclusions regarding the force and response calculations of the heave problem.